Bound and free excitons in ZnO. Optical selection rules in the absence and presence of Time Reversal Symmetry

by

Prime Niyongabo

Submitted in partial fulfilment of the requirements for the degree

Magister Scientiae

in the faculty of Natural Science and Agricultural Science
University of Pretoria
Pretoria

Supervisor: Prof H. W Kunert

May 20, 2009

I declare that the dissertation, which I hereby submit for the degree Magister Scientae at the University of Pretoria, is my own work and has not previously been submitted by me for a degree at this or any other tertiary institution.

Acknowledgements

I would like to thank the following peaple:

My supervisor Prof. H. W. Kunert and Mr Machatine for expert guidance, for being understanding and for being a great source of advice and inspiration.

My parents for their inspiring encouragements, love and assistance through my years of studies.

My wife Janviere, my daughter Guegue and my son Brillant for encouragements, patience and support.

My colleagues of Honors lab especially Louwrens Van Schalkwyk, for helping me with numerous things with LaTeX.

Summary

The study is focused on finding the origins of optical transitions from ZnO doped by the impurities such as Li, Al, Ga and In using ordinary photoluminescence and magneto-photoluminescence spectroscopy.

We have employed group theoretical methods to study the symmetry of these free dopants before and after putting into the ZnO crystalline field. The group theory allows the classification of the states of dopants in the crystalline field. The symmetry of the free atoms is full rotational group which is reduced to the symmetry operators of the point group of ZnO when they are put into ZnO crystal. The states of these dopants are doublets (2s+1=2) and exhibit anomalous Zeeman splitting. In ZnO, these dopants become shallow donors (Al, Ga and In) to which excitons of symmetries $\Gamma_7^c \oplus \Gamma_7^v$(A), $\Gamma_7^c \oplus \Gamma_9^v$(B) and $\Gamma_7^c \oplus \Gamma_7^v(C)$ are bound.

We have demonstrated a correlation between ionized and neutral donor bound excitons of the same chemical identity in ZnO. For greater understanding of these excitonic transitions, we have studied the electronic band structure of ZnO and established the excitonic selection rules in the absence and presence of time reversal symmetry (TRS). We have proven that the inclusion of TRS does not change the existing selection rules compared to those in the absence of TRS. Only, it introduces new states of the same symmetry.

Contents

List of Tables

List of Figures

1 Introduction

The excitonic state of a crystal is an excited state of the whole crystal and thus the electron-hole pair is mobile and can move throughout the lattice. In semiconductors, such as the III-VI compound crystals, the electron-hole pairs are loosely bound and are called Wannier excitons. However, in insulators such as the alkali-halides and alkali earth fluorides the excitons are tightly bound electron-hole pairs. These excitons exhibit more local atomic character and are termed Frenkel excitons.

1.1 Free excitons

The valence band is split into three bands due to the influence of crystal-field and spin-orbit interactions. The near-band-gap intrinsic absorption and emission spectrum is dominated by transition from these three valence bands. The related free-exciton transitions from the conduction band to these three valence bands or vice versa are usually denoted by A (also referred to as the heavy hole), B (also referred to as the light hole), and C (also referred to as the crystal-field split band). Recent availability of high-quality ZnO single crystals has paved the way to observe intrinsic exciton transitions in low temperature photoluminescence (PL), magnetoluminescence, and reflectance measurements. However, the ordinary PL technique can only probe A-excitons at k = 0 of symmetries Γ_5 and $\Gamma_6(\Gamma_7^c \otimes \Gamma_9^c = \Gamma_5 \oplus \Gamma_6 = \Gamma_5(\uparrow\downarrow) + \Gamma_6(\uparrow\uparrow))$. The shoulder lines at around 3.3750eV and 3.3775eV might be related to Γ_5(anti-parallel spins) and Γ_6 (parallel spins) respectively Fig.15.

1.2 Bound excitons

By the term bound exciton is meant an electronic excitation of a crystal in which an electron-hole pair is localized near an imperfection in the crystal. Bound excitons are extrinsic transitions and are related to dopants and defects, which usually create electronic states in the band gap, and therefore influence both optical-absorption and emission processes. They are observed as sharp-line optical transitions in photoluminescence. The excitons could be bound to neutral donor or acceptor to form molecular states, or to ionized donor or acceptor to form molecular ion states. In high-quality bulk ZnO substrates, the neutral shallow donor bound excitons (DBE) often dominate because of the presence

Table 1: Free and bound exciton recombinations. A_L and A_T are the longitudinal and transversal free A-exciton states. A_T is the reference for the determination of the bound exciton localisation energy.

Line	Wavelength (nm)	Energy (eV)	Localisation energy(meV)	Donor binding energy(meV)	Chemical identity
A_l	367.12	3.3772			
A_T	367.26	3.3759			
I_0	367.63	3.3725	3.4		
I_1	367.71	3.3718	4.1		
I_{1a}	368.13	3.3679	8.0		
I_2	368.19	3.3674	8.5		
I_3	368.29	3.3665	9.4		
I_{3a}	368.34	3.3660	9.9		
I_4	368.34	3.3628	13.1	46.1	H
I_5	368.86	3.3614	14.5		
I_6	368.92	3.3608	15.1	51.55	Al
I_{6a}	368.96	3.3604	15.5	53	
I_7	369.01	3.3600	15.9		
I_8	369.03	3.3598	16.1	54.6	Ga
I_{8a}	369.08	3.3593	16.6		
I_9	369.37	3.3567	19.2	63.2	In

of donors due to unintentional (or dopant) impurities and/or shallow donorlike defects. In samples containing acceptors, the acceptor bound excitons (ABE) are observed.

Fig.15 shows two types of exciton complexes related to impurities in ZnO: Neutral donor-bound exciton (I_{6a}, I_7, I_8 and I_9) and ionized donor-bound excitons (I_0, I_1 and I_2). Table 1 shows the free and bound excitons with their localisation energies and chemical identities.

The studies of these lines are carried out by means of Zeeman spectroscopy. It is our aim to develop briefly the theory of the Zeeman effect.

The Zeeman effect denotes the splitting of the spectral lines emitted by atoms located in a magnetic field. This effect was first observed in 1896 by Zeeman . Lorentz found a classical explanation of this effect, according to which each spectral line of an atom should split into three components [1]. This Lorentz triplet was referred to as the normal Zeeman effect (NZEef). Many atoms were also found whose spectral lines split into more complicated structures, this effect was named the anomalous Zeeman effect (AnZEef).

The said effect could only be explained with the help of the hypothesis of electron spin, which was formulated in 1925 by Goudsmit and Uhlenbeck. This success ultimately contributed to the general acceptance of the theory of electron spin and the associated intrinsic magnetic moment of the electron.

The Zeeman effect leads to many applications:

In experimental spectroscopy, by analyzing the splittings of the spectral lines of an atom, the spectroscopist can determine the splittings of the energy levels of the atoms ($\mu_\beta \mathbf{Bg}$).

The most easily interpreted evidence for the splitting of atomic energy levels in an external magnetic field is electron spin resonance (ESR)[2]. If atoms in their ground state are placed in a region containing electromagnetic radiation of frequency ν, and a steady magnetic field $\mathbf{B}$ is applied to the region, the electromagnetic energy will be strongly absorbed when the photons have energy $h\nu$ which just equals the Zeeman splitting of the two components of the ground state energy level. The photons are able to induce transitions between the components in which they are absorbed.

A type of Zeeman effect can also be observed in the hyperfine structure when the nucleus and spin are interacting.

In Magnetophotoluminescence, the Zeeman effect measurement leads to impurity and exciton complexes analysis in a semiconductor with greater confidence and accuracy in a strong magnetic field. Indeed, the pholuminescence peaks of the spectrum corresponding to exciton bounds for impurities are due to optical transitions. The relative intensities of these peaks in the spectra reflect the relative concentration of impurities of the semiconductor[3].

In magnetoabsorption, the Zeeman measurement provides information about the band structure of a semiconductor. This involves the transitions between the valence band and the conduction band as well as between the valence band and the bound exciton levels.

The Zeeman effect associated with magnetoabsorption will also furnish information about transitions between the degenerate and the split-off bands in a semiconductor[4]. It is our aim to study the optical properties of ZnO doped with Lithium by means of low temperature photoluminescence and magneto-photoluminescence.

The organisation of the present thesis is as follows:

The first section introduced the thesis with an oveview of free and bound excitons in ZnO.

In the second section, an atom in an external magnetic field is discussed and the observed normal and anomalous Zeeman effects is studied. The spectral terms of free atoms: Li, Al, Ga and In dopants of ZnO are given and by employing the group theory we demonstrate how the atomic levels of the Li, Al, Ga and In split in the crystalline field of ZnO.

In section three we describe the band structure of the wurtzite ZnO at k = 0 and study the selection rules in the absence and presence of Time Reversal Symmetry.

In section four the experimental results are discussed.

Section five concludes the thesis with a brief summary followed by the reference list and appendix.

2 An atom in an external magnetic field

In this section, we briefly recall the classical theory of the normal Zeeman effect with regards to an atom placed in an external magnetic field. We study the effect of an external magnetic field on spectral terms of free atoms. In order to analyse the ordinary Photoluminescence and Magnetophotoluminescence (PL, MPL) spectra, we also recall the theories of NZEef and the AnZEef.

2.1 Normal Zeeman effect

The normal Zeeman effect disregards the spin of the electrons and consequently the spin-orbit and spin-spin interactions are not taken into account.

An atom in a magnetic field can be modelled as a simple harmonic oscillator. The restoring force on the electron is the same for the displacements in all directions and the oscillator has the same resonance frequency ω_0 for motion along the x,y, and z directions (when there is no magnetic field). In magnetic field $\mathbf{B}$ the equation of motion for an electron with charge $-e$, position r and velocity $v = \dot{r}$ is:

$$m_e \frac{d\vec{\mathbf{v}}}{dt} = -m_e \omega_0^2 \vec{\mathbf{r}} - e\vec{\mathbf{v}} \times \mathbf{B} \tag{1}$$

With

$$\vec{\mathbf{r}} = \vec{\mathbf{r}}_0 e^{-i\omega t} \tag{2}$$

Substituting eq. 2 into 1, we obtain the frequencies: $\omega = \omega_o, \omega = \omega_o - \Omega_L, \omega = \omega_o + \Omega_L$ of the electrons oscillating along the x,y and z axes in a magnetic field: see appendix A and Figs.1, 2.

An electron in a free atom, when there is no external perturbation applied, does not emit light. When external steady state magnetic field $\mathbf{B}$ is applied, the oscillating electron acts as a classical dipole and emits the radiative electromagnetic waves. In other words the external magnetic field induces in an atom a dipole moment. It is shown by calculations and experimental spectra that the emitted light consists of three different frequencies.

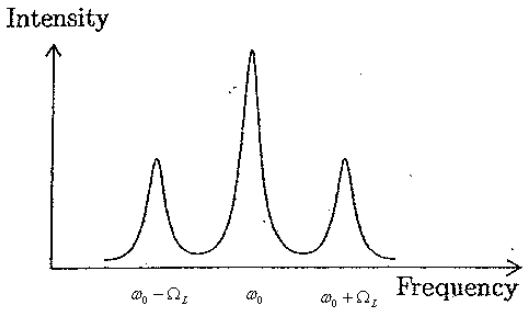

Figure 1: For the normal Zeeman effect, a simple model of an atom explains the frequencies of the light emitted : $\omega_0 - \Omega_L$,ω_0, and $\omega_0 + \Omega_L$

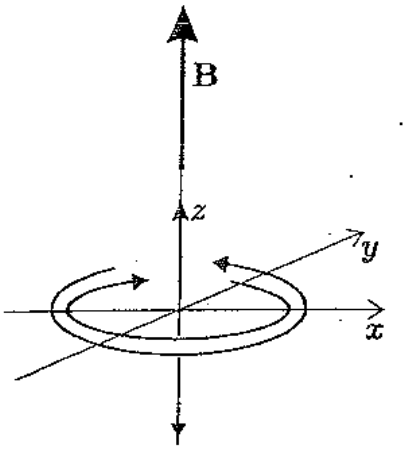

Figure 2: A simple model of an atom as an electron that undergoes simple harmonic motion explains the features of the Zeeman effect of a magnetic field (along the z-axis).The three eigenvectors of the motion are:$\hat{e}_z cos\omega_0 t$ and $cos(\{\omega_0 \pm \Omega_L\}\, t)\hat{e_x} \pm sin(\{\omega_0 \pm \Omega_L\}\, t)\hat{e_y}$

The magnetic field does not affect the motion along the z axis and the angular frequency of the oscillator remains ω_o. The interaction with the magnetic field causes the motions in the x and y directions to be coupled together. This results in two circular motions in opposite directions in the xy plane, as illustrated in Fig 2. These circular motions have frequencies shifted up, or down, from ω_o by the Larmor frequency.

This classical model of the Zeeman effect explains the polarisation of light as well as the splitting of the lines into three components. The calculation of the polarization of the radiation at each of the three different frequencies for the general direction of the observation is straightforward using vectors. However, only the particular cases where the radiation propagates parallel and perpendicular to the magnetic field are considered: the longitudinal and transverse directions of the observation respectively. The π-component of the line is observed in all directions except along the magnetic field. The σ- components in contrast to the π- components are seen in the longotudinal observation Fig.3 and 4.

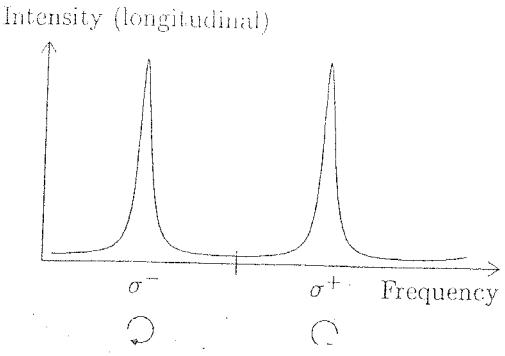

Figure 3: For the normal Zeeman effect, a simple model of an atom explains the frequency of the light emitted and its polarization indicated by the arrows for transverse observations

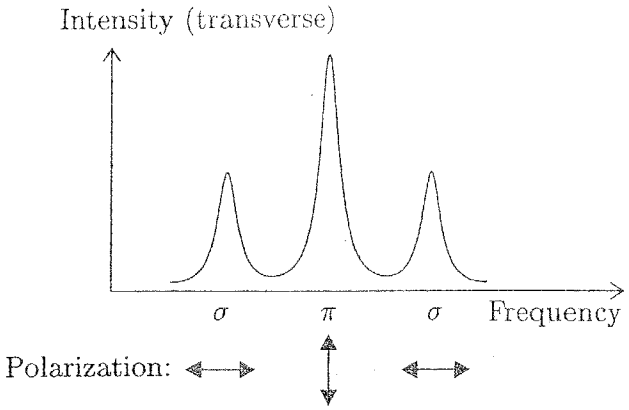

Figure 4: For the normal Zeeman effect, a simple model of an atom explains the frequency of the light emitted and its polarization indicated by the arrows for the cases of longitudinal observation

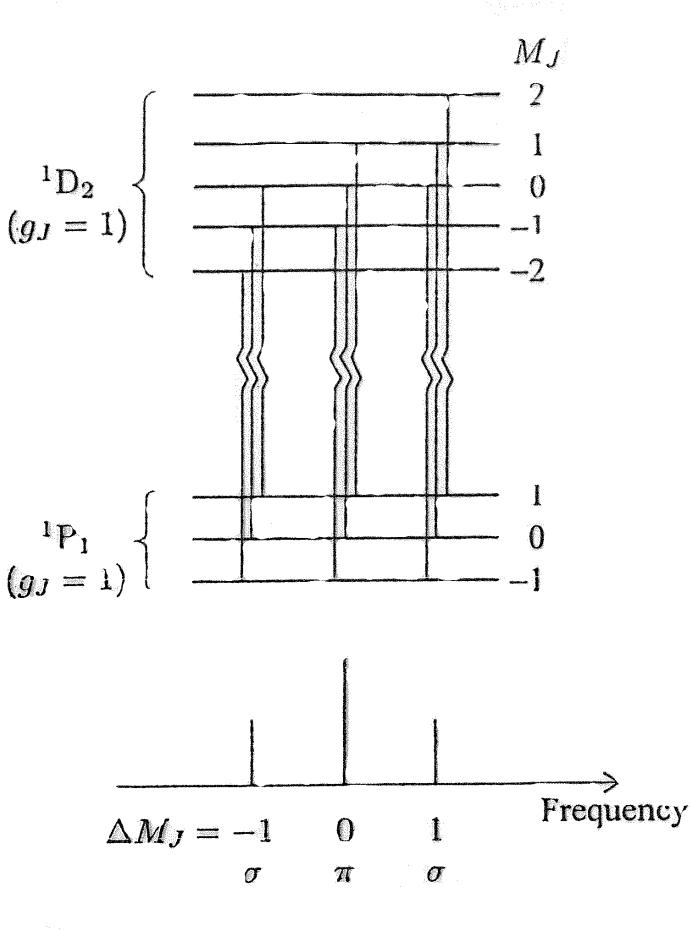

Figure 5: Term diagram of normal Zeeman effect

Fig.5 dipects the normal Zeeman effect on the $1s2p^1P - 1s3d^1D_2$ line in helium. These levels split into three and five m_j states respectively. Both levels have s = 0 and g = 1 so that the allowed transitions between the states create the same pattern of three components as the classical model. This is the historical reason why it is termed the normal Zeeman effect. Any other pattern is called the anomalous Zeeman effect, although such patterns have a direct explanation in quantum mechanics and arise whenever $S \neq 0$. e.g. all atoms with one valence electron have $S = \frac{1}{2}$. The π- and σ-components arise from $\Delta m_j = 0$ and $\Delta m_j = \pm 1$ transitions, respectively. The positions of the energy levels of the atom are given by the relation:

$$E = m_l \mu_\beta g B \tag{3}$$

With m_l, the orbital magnetic moment, μ_β, the Bohr magneton $= e\hbar/2mc$, g the Landé factor from Fig.5 g = 1(See Eq. 8 section 2.31).

The Figs. 3, 4 show the frequency of light emitted and its polarization. Fig.5 illustrates the selection rules governing the transitions between the states.

2.2 Selection rules for optical transitions in free atoms

The selection rules that govern allowed transitions arise from the angular integral

$$\tau_{ang} = \int_0^{2\pi} \int_0^{\pi} Y^*_{l_2,m_2}(\theta,\phi)\hat{r}\cdot\hat{e}_{rad}Y_{l_1,m_1}(\theta,\phi)\sin\theta d\theta d\phi \tag{4}$$

which contains the angular dependence of the interaction $\hat{r}\cdot\hat{e}_{rad}$ for a given polarisation of the radiation. The mathematics requires that we calculate τ_{ang} for an atom with a well-defined quantisation axis and radiation that has a well-defined polarization and direction of propagation. This corresponds to the physical situation of an atom experiencing the Zeeman effect of an external magnetic field and indicates that treatment of the electron as a classical oscillator showed that the components of different frequencies within the Zeeman pattern have different polarisations. We employ the same nomenclature of π- and σ-transitions here. Transverse observation refers to radiation emitted perpendicular to the magnetic field, and longitudinal observation lies along the z-axis.

1. *π- transitions*

   These are transitions arising from the transverse observations referring to radiations emitted perpendicular to the magnetic field. For this polarisation the magnetic quan-

tum number does not change, $\Delta m_l = 0$.

2. *σ-transitions*

   These are transitions arising from the longitudinal observations referring to radiations emitted along the magnetic field (z-axis). For this polarisation, the magnetic quantum number changes, and the selection rule is $\Delta m_l, = \pm 1$. where the m_l is the orbital magnetic quantum number.

2.3 The anomalous Zeeman effect

In subsection 2.1 it has been shown that the normal Zeeman effect, which disregards the spin of the electron, can be discribed by the classical Lorentz Theory.
In the anomalous Zeeman effect, the interaction between the electron's spin magnetic dipole moment and the weak magnetic field is taken into account. The total atom's magnetic moment has orbital and spin contributions:

$$\tilde{\mu} = -\tilde{\mu_\beta}\mathbf{L} - \mathbf{g_s}\tilde{\mu_\beta}\mathbf{S} \tag{5}$$

For a single electrons model, e.g. alkali atoms, the Hamiltonian can then be written

$$H = -\frac{\hbar^2}{2m}\nabla^2 + V(r) + \xi(r)\mathbf{L}.\mathbf{S} + \mathbf{B}\gamma_\mathbf{0}(\mathbf{L_z} + \mathbf{2S_z}) \tag{6}$$

with $\gamma_0 = e/2mc$, where the first two terms of the Hamiltonian describe the kinetic and potential energy respectively, the third term describes the spin-orbit interaction, and the last term describes the Zeeman effect.
The interaction of the atom with the external magnetic field is described by $H_{ZE} = -\mu.\mathbf{B}$
In the vector model the magnetic moment is projected along J (see Fig.6).

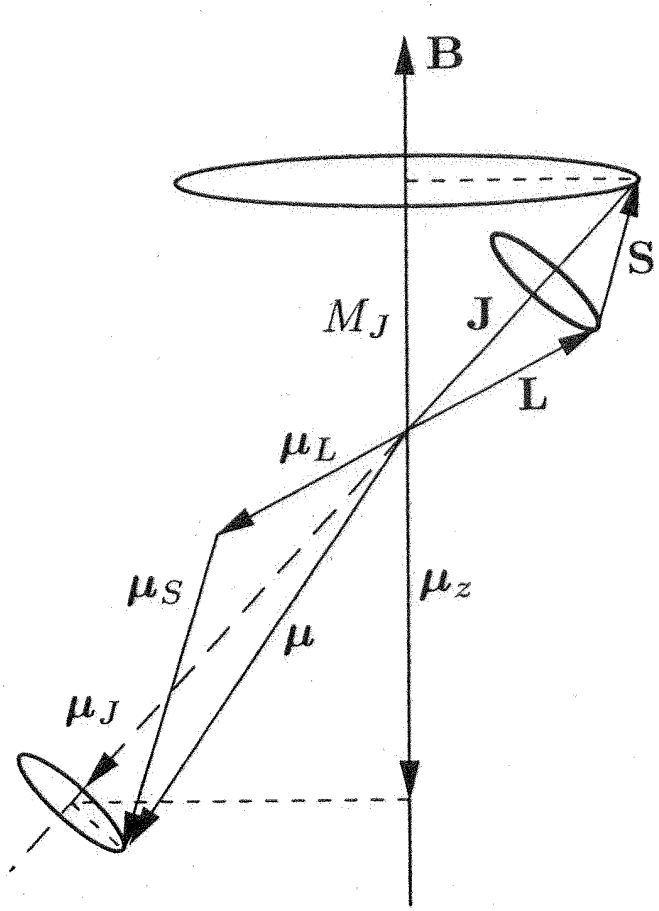

Figure 6: The contributions to the total magnetic moment from the motion and spin are projected along J.

The Zeeman energy is :

$$E_{ZE} = g_j \mu_B \mathbf{B} \mathbf{M_J} \tag{7}$$

Where the landé $g-$ factor is (See Appedix B for rigid derivation)

$$g_J = \frac{3}{2} + \frac{s(s+1) - l(l+1)}{2j(j+1)} \tag{8}$$

and the $\mu_\mathbf{B} = \mathbf{eh/2mc}$ is the Bohr magneton. Fig.7 dipects the typically term diagram of the anomalous Zeeman effect.

The singlet terms have S $= 0$ so $\mathbf{J} = \mathbf{L}$ and g_J. The singlets all displays the same Zeeman splitting between M_J states, and transitions between singlet terms exhibit the normal Zeeman effect Fig.5. The $\Delta M_J \pm 1$ transitions have frequencies shifted by $\pm \mu_\beta \mathbf{B/h}$ with respect to the $\Delta M_J = 0$ transitions. In both the normal and anomalous Zeeman effects the π - transitions ($\Delta M_J = 0$) and σ -transitions ($\Delta M_J = \pm 1$) exhibit the same polarizations as in the classical model. The Zeeman effect observed for $2^P_{\frac{1}{2}} -^2 S_{\frac{1}{2}}$ and $2^P_{\frac{1}{2}} -^2 S_{\frac{1}{2}}$ transitions that arise between the fine-structure components of the alkalis is shown in Fig.7.

For example, we can consider the emission due to electric dipole transitions between an excited p-state and a ground s-state. The energy level with and without a magnetic field are shown in Fig. 7. The ground state is $S_{\frac{1}{2}}(J=\frac{1}{2})$ and splits into two Zeeman levels for $m_j = \pm\frac{1}{2}$ while p-state is split by spin-orbit coupling into two states $P_{\frac{3}{2}}(j=\frac{3}{2})$ and $P_{\frac{1}{2}}(J=\frac{1}{2})$ which are then further split by the magnetic field into a quartet, $m_j = \pm\frac{3}{2}, \pm\frac{1}{2}$, and doublet, $m_j = \pm\frac{1}{2}$. The allowed transitions are also shown and are of two types; there are σ transitions for $m_j = \pm 1$ which give rise to luminescence which is circularly polarized, when observed parallel to the magnetic field or linearly polarized perpendicular to B if observed normal to B. There are also π transitions for $m_j = 0$ which give radiation linearly polarized parallel to the magnetic field when observed normal to it.

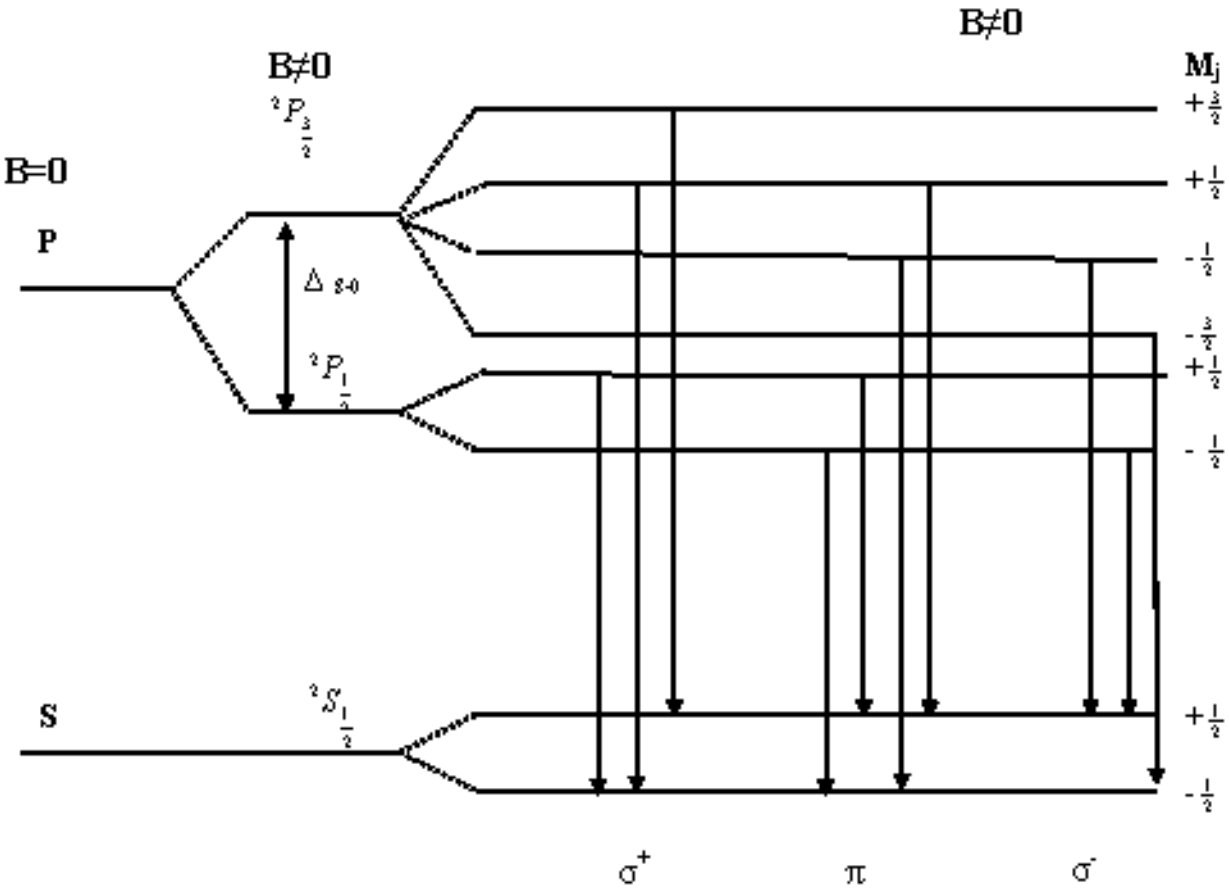

Figure 7: Energy level diagram showing the allowed transitions between a p-state and an s-state in the presence of a magnetic field. The transitions are grouped according to the polarizations,σ_+, π and σ_-.

In the next section we will discuss the magneto-photoluminescence spectral for ZnO-Li, in terms of the theory discussed here.

2.4 Spectral terms of free atoms: Li, Ga, Al, and In dopants of ZnO crystal

2.4.1 Electronic configuration of Li, Ga, Al, and In

The ground states of these elements displays the following electronic configurations [5]:

Table 2: The Electronic Configurations of the Li, Al, Ga and In

Shell	K	L	M	N	Q	Normal
n	1	2	3	4	5	state
Subshell (l)	0 1	0 1	0 1 2	0 1 2	0 1	
Li	$1s^2$	2s				$^2S_{\frac{1}{2}}$
Al	$1s^2$	$2s^2$ $2p^6$	$3s^2$ 3p			$^2P_{\frac{1}{2}}$
Ga	$1s^2$	$2s^2 2p^6$	$3s^2 3p^6 3d^0$	$4s^2$ 4p		$^2P_{\frac{1}{2}}$
In	$1s^2$	$2s^2 2p^6$	$3s^2 3p^6 3d^{10}$	$4s^2$ $4p^6 4d^{10}$	$5s^2$ 5p	$^2P_{\frac{1}{2}}$

2.4.2 Spectroscopic nomenclature of free atoms

In general, the spectroscopic nomenclature of free atoms consists of the ${}^{2S+1}\mathrm{X}_J$ symbols, where:

- $2S+1$ stands for the spin degeneracy
- $\mathrm{X} \Rightarrow$ L $\Rightarrow$ S, P, D, F, $\cdots$ stands for the orbital angular momentum
- S stands for the total spin of the free atom
- $J = L + S$, stands for the total angular momentum.

The spectroscopic nomenclatures of Li and Al elements are listed below:

- For Li : ${}^2S_{\frac{1}{2}} \Rightarrow$ S $\Rightarrow$ L $= 0$; $2 = 2S+1$, $S = \frac{1}{2}$; J = L $\pm S = \frac{1}{2}$
- For Al : ${}^2P_{\frac{1}{2}}$ and ${}^2P_{\frac{3}{2}} \Rightarrow$ P $\Rightarrow$ L$= 1$, $2 = 2S+1$, $S = \frac{1}{2}$; J = L $\pm$ S $\Rightarrow \frac{1}{2}, \frac{3}{2}$.

Let us consider the Li element and determine the possible spectral terms. The ground state is : $1S^2 2S$.
For $1S^2$ terms; $n = 1$, $l = 0$, $s = 0$;
For $2S$ terms; $n = 2, l = 0, s = \frac{1}{2}$ and the spectral term is ${}^2S_{\frac{1}{2}}$.
The shell $1S^2$ with zero total spin zero and no angular momentum $l = 0$ is totally fullfilled and does not contribute to excited states of Li.
Therefore, $2S$ shell alone will contribute to the excited states by increasing the n and l quantum numbers.
Consider $n = 2, l = 1, s = \frac{1}{2}$ for the L shell (see table 1): $J = 1 \pm \frac{1}{2}$; the spectral terms are: ${}^2P_{\frac{1}{2}}$ and ${}^2P_{\frac{3}{2}}$.
Consider $n = 3, l = 2, s = \frac{1}{2}$ for M shell : $j = 2 \pm \frac{1}{2}$, the spectral terms are: ${}^2D_{\frac{3}{2}}$ and ${}^2D_{\frac{5}{2}}$.
Consider $n = 4, l = 3, s = \frac{1}{2}$ for the N shell : $j = 3 \pm \frac{1}{2}$; the spectral terms are: ${}^2F_{\frac{5}{2}}$ and ${}^2F_{\frac{7}{2}}$ etc.
Because from the ground state to the excited states the total spin remains half ($s = \frac{1}{2}$), the terms are doublets. Therefore, the normal triplet Zeeman effect can not be observed in Li, Ga, Al, and In.
The normal state $2s$ arises from the electron configuration $1s^2 2s$. If the atom is to be excited now, the last bound and most easily moved electron $2s$ may potentially move to any of the higher states, for example to $2p, 3s, 3p, 3d, 4s, 4p$ etc...

If the excited electron is in the $3d$ state, for example, the complete electron configuration of the atom is designated as $1s^2 3d$ and the energy level as 3^2D.

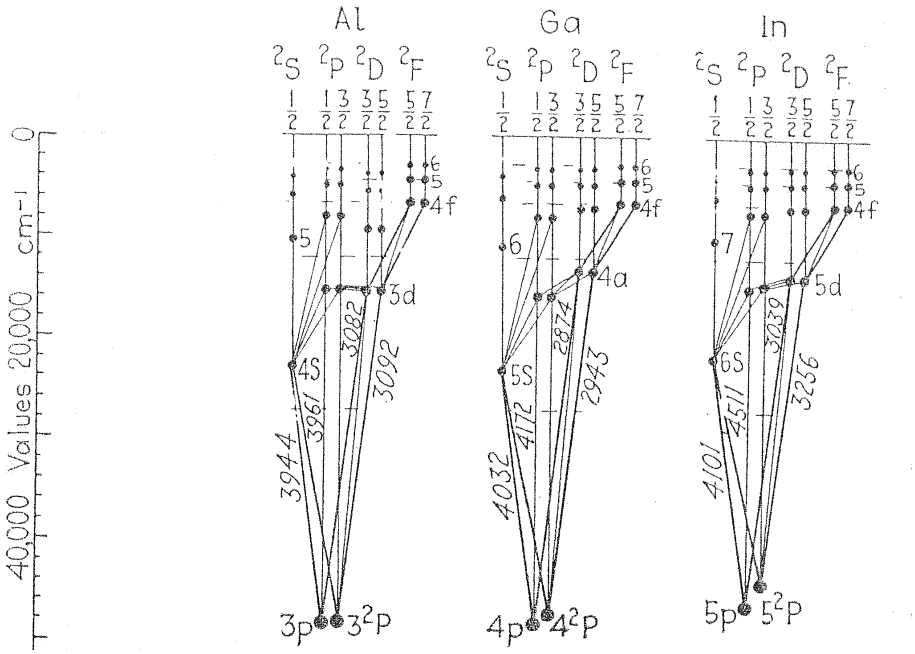

Figure 8: Energy level diagrams of the Al, Ga, and In

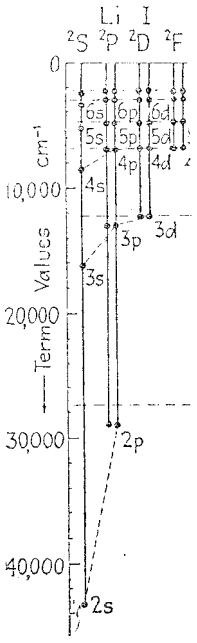

Figure 9: Energy level diagram of li

2.4.3 Absorption and emission experimental spectra of the free atoms

Energy levels of the free atoms have been measured experimentally by absorption and emission and are shown in Fig.8. The localisation energies for different transitions between the states are calculated Figs.8, 9 and listed in tables 3-6.

Table 3: Transitions and Localisation energy for Al

Transitions	Wavelength($\dot{A}$)	Localisation energy(eV)
3p - 4s	3944	3.144
3p - 3d	3082	4.023
3^2p - 4s	3961	3.130
3^2p - 3d	3092	4.010

Table 4: Transitions and Localisation energy for Ga

Transitions	Wavelength($\dot{A}$)	Localisation energy(eV)
4p - 4s	4032	3.075
4p - 4d	2874	4.314
4^2p - 5s	4172	2.972
4^2p - 4d	2943	4.213

Table 5: Transitions and Localisation Energy for In

Transitions	Wavelength($\dot{A}$)	Localisation Energy(eV)
5p -6s	4101	3.023
5p - 5d	3039	4.079
5^2p - 6s	4511	2.745
5^2p -5d	3256	3.808

Table 6: Transitions and Localisation energy for Li

Transitions	Wavelength($\dot{A}$)	Localisation Energy(eV)
2s -3s	3676	3.373
2p - 3p	6242	1.986
3d - 4d	18742	0.662
4f-5f	40415	0.307

2.5 Group theoretical classifications of free atomic levels.

In this section we investigate the symmetry of free atoms before being planed into a crystal. In particular, we are interested in the classification of states of spectral terms of atoms. Theafter, we study the effect of the crystalline field on the spectral terms of an atom or ion in a crystal.

1. **Symmety of a free atom**

   The full rotation group of a free atom follows the solution of the Laplace equation [6].

   $$\nabla^2\psi = 0 \tag{9}$$

   The transformation (rotation) which takes the points in a three-dimentional space from their initial to their final positions is described in terms of Euler angles α, β, γ and the operators of the full rotation group (FRGr) are $\hat{O}_R(\alpha, \beta, \gamma)$. These are continuous and infinite groups.

   The basis for the operators $\hat{O}_R(\alpha, \beta, \gamma)$ is the well known spherical harmonics $Y^l_m(\theta, \phi)$. The representations are obtained from:

   $$\hat{O}_R(\alpha, \beta, \gamma)Y^l_m(\theta, \phi) = \sum_{m'} Y^l_m(\theta, \phi)D^l_{m',m}(\alpha, \beta, \gamma) \tag{10}$$

   Where l is the orbital angular momentum quantum number, $m_l = -l, ..., +l$ is the orbital magnetic moment quantum number and $D^l_{m',m}(\alpha, \beta, \gamma)$ is the matrix of R(α, β, γ) in the representation D^l based on the spherical harmonics of order l.

   The representations D^0, D^1, D^2,... etc constitute a complete set of single-valued irreducible representations and

   $$D^l_{m'm}(\alpha, \beta, \gamma) = e^{-im'\gamma}d^l_{m'm}(0, \beta, 0)e^{-im\alpha} \tag{11}$$

   where the matrix elements of $d^l(\beta)$ are:

   $$\begin{aligned} d^l_{m',m}(\beta) &= \sum_t (-1)^t \frac{\sqrt{(l+m')!(l-m')!(l+m)!(l-m)!}}{(l+m'-t)!(l-m-t)!(t+m-m')!} \\ &\times \left(\cos\frac{\beta}{2}\right)^{2l+m'-m-2t} \cdot \left(\sin\frac{\beta}{2}\right)^{2t+m-m'} \end{aligned} \tag{12}$$

and the sum is taken over all values of t which lead to nonnegative factorials.

For instance $D^l_{m'm}$ for l = 1 and m,m'; -1, 0, 1: using Eq.12, we obtain

$$D^1_{m'm}(\alpha,\beta,\gamma) = \begin{pmatrix} e^{-i\alpha}\frac{1+\cos\beta}{2}e^{-i\gamma} & -e^{-i\alpha}\frac{\sin\beta}{\sqrt{2}} & e^{-i\alpha}\frac{1-\cos\beta}{2}e^{i\gamma} \\ \frac{\sin\beta}{\sqrt{2}}e^{-i\gamma} & \cos\beta & -\frac{\sin\beta}{\sqrt{2}}e^{i\gamma} \\ e^{i\alpha}\frac{1-\cos\beta}{2}e^{-i\gamma} & e^{i\alpha}\frac{\sin\beta}{\sqrt{2}} & e^{i\alpha}\frac{1+\cos\beta}{2}e^{i\gamma} \end{pmatrix} \tag{13}$$

When the symmetry of the FRG $\hat{O}(\alpha,\beta,\gamma))$ is reduced to C_6 point group we have $\alpha = \gamma = 0$ and $\beta = \phi = 0, \frac{\pi}{3}, \frac{2\pi}{3}, \pi, \frac{4\pi}{3}, \frac{5\pi}{3}$ (see Fig.10). In other words $D^l(0,\beta,0)$ will be one of the irrps of C_6. The characters of $D^l(0,\beta,0)$ will depend on the angle of rotation ϕ as will be demonstrated later. It follows that if l =1

$$D^1(\beta) = d^1_{m'm}(\beta) = \begin{pmatrix} d^1_{11} & d^1_{10} & d^1_{1-1} \\ d^1_{01} & d^1_{00} & d^1_{0-1} \\ d^1_{-11} & d^1_{-10} & d^1_{-1-1} \end{pmatrix} \tag{14}$$

where:

$$\begin{aligned} d^1_{11} &= d^1_{-1-1} = \cos^2(\frac{\beta}{2}) \\ d^1_{1-1} &= d^1_{-11} = \sin^2(\frac{\beta}{2}) \\ d^1_{01} &= d^1_{-10} = -d^1_{0-1} = -d^1_{10} = \frac{\sin\beta}{\sqrt{2}} \\ d^1_{00} &= \cos\beta \end{aligned} \tag{15}$$

For the six angles we obtain a set of six matrices 3×3 which is one of the reduced SV representations of C_6 in the hexagonal basis shown in Fig. 10.

Similarly for l = 2, (m, m' -2, -1, 0, 1, 2,), we obtain the irreducible representation

of the full rotation group.

$$D^2_{m'm}(\alpha,\beta,\gamma) = \begin{pmatrix} e^{-2i\alpha}d^2_{22}e^{-2i\gamma} & e^{-2i\alpha}d^2_{21}e^{-i\gamma} & e^{-2i\alpha}d^2_{20} & e^{-2i\alpha}d^2_{2-1}e^{i\gamma} & e^{-2i\alpha}d^2_{2-2}e^{2i\gamma} \\ e^{-i\alpha}d^2_{12}e^{-2i\gamma} & e^{-i\alpha}d^2_{11}e^{-i\gamma} & e^{-i\alpha}d^2_{10} & e^{-i\alpha}d^2_{1-1}e^{i\gamma} & e^{-i\alpha}d^2_{1-2}e^{2i\gamma} \\ d^2_{02}e^{-2i\gamma} & d^2_{01}e^{-i\gamma} & d^2_{00} & d^2_{0-1}e^{i\gamma} & d^2_{0-2}e^{2i\gamma} \\ e^{i\alpha}d^2_{-12}e^{-2i\gamma} & e^{i\alpha}d^2_{-11}e^{-i\gamma} & e^{i\alpha}d^2_{-10} & e^{i\alpha}d^2_{-1-1}e^{i\gamma} & e^{i\alpha}d^2_{-1-2}e^{2i\gamma} \\ e^{2i\alpha}d^2_{-22}e^{-2i\gamma} & e^{2i\alpha}d^2_{-21}e^{-i\gamma} & e^{2i\alpha}d^2_{-20} & e^{2i\alpha}d^2_{-2-1}e^{i\gamma} & e^{2i\alpha}d^2_{-2-2}e^{2i\gamma} \end{pmatrix} \tag{16}$$

If l = 2 for $\alpha = \gamma = 0$ and $\beta = \phi$, the matrix becomes:

$$d^2_{m'm}(\beta) = \begin{pmatrix} d^2_{22} & d^2_{21} & d^2_{20} & d^2_{2-1} & d^2_{2-2} \\ d^2_{12} & d^2_{11} & d^2_{10} & d^2_{1-1} & d^2_{1-2} \\ d^2_{02} & d^2_{01} & d^2_{00} & d^2_{0-1} & d^2_{0-2} \\ d^2_{-12} & d^2_{-11} & d^2_{-10} & d^2_{-1-1} & d^2_{-1-2} \\ d^2_{-22} & d^2_{-21} & d^2_{-20} & d^2_{-2-1} & d^2_{-2-2} \end{pmatrix} \tag{17}$$

Where

$$\begin{aligned} d^2_{22} &= d^2_{22} = cos^4\frac{\beta}{2} \\ d^2_{21} &= -d^2_{12} = -d^2_{-2-1} = d^2_{-1-2} = -\frac{1}{2}\sin\beta(1+\cos\beta) \\ d^2_{20} &= d^2_{02} = d^2_{-20} = d^2_{0-2} = \sqrt{\frac{3}{8}}\sin^2\beta \\ d^2_{2-1} &= d^2_{1-2} = -d^2_{-21}d^2_{22} = -d^2_{-12} = \frac{1}{2}\sin\beta(\cos\beta - 1) \\ d^2_{2-2} &= d^2_{-22} = \sin^4(\frac{\beta}{2}) \\ d^2_{11} &= d^2_{-1-1} = \frac{1}{2}(2\cos\beta - 1)(\cos\beta + 1) \\ d^2_{1-1} &= d^2_{-11} = \frac{1}{2}(2\cos\beta + 1)(1 - cos\beta) \\ d^2_{10} &= d^2_{0-1} = -d^2_{01} = -d^2_{-10} = -\sqrt{\frac{3}{2}}\sin\beta\cos\beta \\ d^2_{00} &= \frac{1}{2}(3\cos^2\beta - 1) \end{aligned} \tag{18}$$

For j = l + s, the matrix elements of D^j are given by [7]:

$$\begin{aligned} d^j_{m'm}(\beta) &= \sum_t (-1)^k \frac{\sqrt{(j+m)!(j-m)!(j+m')!(j-m')!}}{(j+m-k)!(j-m'-k)!(k+m'-m)!} \\ &\times \left(\cos\frac{\beta}{2}\right)^{2j-m'+m-2k} \cdot \left(-\sin\frac{\beta}{2}\right)^{2k+m'-m} \end{aligned} \tag{19}$$

where the sum is taken over all values of k which lead to non negative factorials.

In case of $j = \frac{1}{2}(m, m' : \frac{1}{2}, -\frac{1}{2})$ the matrix elements of d^j becomes:

$$D^{\frac{1}{2}}_{m'm}(\alpha,\beta,\gamma) = \begin{pmatrix} e^{\frac{-i(\alpha+\gamma)}{2}}\cos\frac{\beta}{2} & -e^{\frac{-i(\alpha-\gamma)}{2}}\sin\frac{\beta}{2} \\ e^{\frac{i(\alpha-\gamma)}{2}}\sin\frac{\beta}{2} & e^{\frac{i(\alpha+\gamma)}{2}}\cos\frac{\beta}{2} \end{pmatrix} \tag{20}$$

Again, for the six angles we obtain a set of six matrices 2×2 which is one of the reduced DV representations of C_6 in the hexagonal basis shown in Fig. 10.
As earlier discussed, the matrix of $D^j(\beta)$ with $\beta = \phi$ will be one of the irrps of C_6 and the characters will depend on the angle ϕ.

$$d^{\frac{1}{2}}_{m'm}(0,\beta,0) = \begin{pmatrix} d^{\frac{1}{2}}_{\frac{1}{2}\frac{1}{2}} & d^{\frac{1}{2}}_{\frac{1}{2}-\frac{1}{2}} \\ d^{\frac{1}{2}}_{-\frac{1}{2}\frac{1}{2}} & d^{\frac{1}{2}}_{-\frac{1}{2}-\frac{1}{2}} \end{pmatrix} \tag{21}$$

where

$$\begin{aligned} d^{\frac{1}{2}}_{\frac{1}{2}\frac{1}{2}} &= d^{\frac{1}{2}}_{-\frac{1}{2}-\frac{1}{2}} = \cos\frac{\beta}{2} \\ d^{\frac{1}{2}}_{-\frac{1}{2}\frac{1}{2}} &= -d^{\frac{1}{2}}_{\frac{1}{2}-\frac{1}{2}} = \sin\frac{\beta}{2} \end{aligned} \tag{22}$$

and for $j = \frac{3}{2}(m, m' : \frac{3}{2}, \frac{1}{2}, \frac{-1}{2}, \frac{-3}{2})$ we have:

$$D^{\frac{3}{2}}(0,\beta,0) = d^{\frac{3}{2}}_{m'm}(\beta) = \begin{pmatrix} d^{\frac{3}{2}}_{\frac{3}{2}\frac{3}{2}} & d^{\frac{3}{2}}_{\frac{3}{2}\frac{1}{2}} & d^{\frac{3}{2}}_{\frac{3}{2}\frac{-1}{2}} & d^{\frac{3}{2}}_{\frac{3}{2}\frac{-3}{2}} \\ d^{\frac{3}{2}}_{\frac{1}{2}\frac{3}{2}} & d^{\frac{3}{2}}_{\frac{1}{2}\frac{1}{2}} & d^{\frac{3}{2}}_{\frac{1}{2}\frac{-1}{2}} & d^{\frac{3}{2}}_{\frac{1}{2}\frac{-3}{2}} \\ d^{\frac{3}{2}}_{\frac{-1}{2}\frac{3}{2}} & d^{\frac{3}{2}}_{\frac{-1}{2}\frac{1}{2}} & d^{\frac{3}{2}}_{\frac{-1}{2}\frac{-1}{2}} & d^{\frac{3}{2}}_{\frac{-1}{2}\frac{-3}{2}} \\ d^{\frac{3}{2}}_{\frac{-3}{2}\frac{3}{2}} & d^{\frac{3}{2}}_{\frac{-3}{2}\frac{1}{2}} & d^{\frac{3}{2}}_{\frac{-3}{2}\frac{-1}{2}} & d^{\frac{3}{2}}_{\frac{-3}{2}\frac{-3}{2}} \end{pmatrix} \tag{23}$$

where

$$\begin{aligned} d^{\frac{3}{2}}_{\frac{3}{2}\frac{3}{2}} &= d^{\frac{3}{2}}_{-\frac{3}{2}-\frac{3}{2}} = \cos^3\frac{\beta}{2} \\ d^{\frac{3}{2}}_{\frac{3}{2}\frac{1}{2}} &= d^{\frac{3}{2}}_{\frac{-1}{2}\frac{-3}{2}} = -d^{\frac{3}{2}}_{\frac{1}{2}\frac{3}{2}} = -d^{\frac{3}{2}}_{\frac{-3}{2}\frac{-1}{2}} = -\sqrt{3}\cos^2\frac{\beta}{2}\sin\frac{\beta}{2} \\ d^{\frac{3}{2}}_{\frac{3}{2}\frac{-1}{2}} &= d^{\frac{3}{2}}_{\frac{-1}{2}\frac{3}{2}} = d^{\frac{3}{2}}_{\frac{1}{2}\frac{-3}{2}} d^{\frac{3}{2}}_{\frac{-3}{2}\frac{1}{2}} = \sqrt{3}\cos\frac{\beta}{2}\sin^2\frac{\beta}{2} \\ d^{\frac{3}{2}}_{\frac{3}{2}\frac{-3}{2}} &= -d^{\frac{3}{2}}_{\frac{-3}{2}\frac{3}{2}} = -\sin^3\frac{\beta}{2} \\ d^{\frac{3}{2}}_{\frac{1}{2}\frac{1}{2}} &= d^{\frac{3}{2}}_{\frac{-1}{2}\frac{-1}{2}} = \cos\frac{\beta}{2}(3\cos^2\frac{\beta}{2} - 2) \\ d^{\frac{3}{2}}_{\frac{1}{2}\frac{-1}{2}} &= -d^{\frac{3}{2}}_{\frac{-1}{2}\frac{3}{2}} = \sin\frac{\beta}{2}(3\sin^2\frac{\beta}{2} - 2) \end{aligned} \tag{24}$$

For the $\phi = 0, \frac{\pi}{3}, \frac{2\pi}{3}, \pi, \frac{4\pi}{3}, \frac{5\pi}{3}$, we have a set of six matrices 4×4 which is one of the reduced DV representations of C_6, that can be decompsed in spinor irreducible representations of C_6.

The above considerations are related to the full spherical symmetry of free atom in cartesian coordinates (x, y, z). However, concerning other coordinate systems like the hexagonal, the meaning of the Euler angles (α, β, γ) will change.

Since the character of a rotation depends only on the angle of rotation and not on the direction of the rotation axis, we can find the characters of d^l as:

$$\chi^l(\phi) = \frac{\sin(l+\frac{1}{2})\phi}{\sin(\frac{\phi}{2})} \tag{25}$$

for SV irrps.

and

$$\chi^j(\phi) = \frac{\sin(j+\frac{1}{2})\phi}{\sin(\frac{\phi}{2})} \tag{26}$$

for DV irrps. Where the angle ϕ is an arbitrary angle of rotation about any direction of the rotation axis.

We have considered the symmetry of free atoms and the classification of their states according to reducible D^l and D^j of the full rotation group. In the next section, we study the splitting of atomic spectral terms due to the crystalline field.

2.6 Splitting of atomic levels of Li, Ga, Al, and In in the crystalline field of ZnO.

Each level of the free atom will belong to one of the irreducible representations of the full rotation group. If an atom is put into a crystal, the electrons will be perturbed by the crystalline field, i.e, by the electric field which is produced at the position of the atom by all other atoms in the crystal, as has been shown in many studies. The electric field will have the symmetry of one of the crystal point groups. In this present case, the levels of unperturbed system will be classified according to the representations of the full rotation group. The level belonging to l -representation will be (2l +1)-fold degeneracy for (SV) irrps and (2j + 1)- fold degeneracy for (DV) irrps [6].

For rotation point groups C_4, C_6, O, etc. the matrices of the FRG, will be reduced to a finite set of matrices which are the reducible representations for the point groups. For example the matrix for C_6 point group will be reduced to the six matrices 3×3 (the reducible representation of C_6).

Similarly, for $\phi = \frac{2\pi}{n}$ we have the forms :

$$\chi^l(\frac{2\pi}{n}) = \frac{\sin(l + \frac{1}{2})\frac{2\pi}{n}}{\sin(\frac{2\pi}{n})} \tag{27}$$

and

$$\chi^j(\frac{2\pi}{n}) = \frac{\sin(j + \frac{1}{2})\frac{2\pi}{n}}{\sin(\frac{2\pi}{n})} \tag{28}$$

For example, using the above equations for C_2, C_3, C_4 and C_6 rotations, we obtain table 7

Table 7: Characters table in (2l+1)-dimensional representation D^l of rotation group

l	0	1	2	3	4	5
$\chi^{(l)}(C_2)$	1	-1				
$\chi^{(l)}(C_3)$	1	0	-1			
$\chi^{(l)}(C_4)$	1	1	-1	-1		
$\chi^{(l)}(C_6)$	1	2	1	-1	-2	-1

for l -integer, and similarly for j -half integer we obtain for D'_4 point group:

For $\phi = 0 : \chi_1 = 2j + 1, \chi_2 = -\chi_1$

For $\phi = \pi : \chi_5 = \chi_6 = \chi_7 = 0$

For $\phi = \frac{\pi}{2} : \chi_3 = \frac{\sin(j+\frac{1}{2})\frac{\pi}{2}}{\sin\frac{\pi}{4}} = \sqrt{2}$, 0 and $\sqrt{2}$ for $j = \frac{1}{2}, (j = \frac{3}{2}, \frac{7}{2})$ and $j = \frac{5}{2}$

$\chi_4 = -\chi_3$

Table 8: Characters table in (2j+1)-dimensional representation D^j of rotation group

j	E	R	C_4^3	C_4^3R	C_4	C_4R	C_2	C_2R	$C_{2'}$	$C_{2'}R$	C_4^2	C_4^2R
$\frac{1}{2}$	2	-2	$-\sqrt{2}$	$\sqrt{2}$	$\sqrt{2}$	$-\sqrt{2}$	0	0	0	0	0	0
$\frac{3}{2}$	4	-4	0	0	0	0	0	0	0	0	0	0
$\frac{5}{2}$	6	-6	$\sqrt{2}$	$-\sqrt{2}$	$-\sqrt{2}$	$\sqrt{2}$	0	0	0	0	0	0
$\frac{7}{2}$	8	-8	0	0	0	0	0	0	0	0	0	0

In case of ZnO the crystal point group is C_6v. The characters for (SV) irrps and (DV) irrps are calculated and tabulated in tables 10 and 12.

For $\phi = 0 : \chi_1 = 2l + 1$

Table 9: Single - Valued Representations of C_{6v}

C_{6v}	E	C_6^3	$C_6^2(2)$	$C_6(2)$	$\sigma_v(3)$	$\sigma_{v'}(3)$
Γ_1	1	1	1	1	1	1
Γ_2	1	1	1	1	-1	-1
Γ_3	1	-1	1	-1	1	-1
Γ_4	1	-1	1	-1	-1	1
Γ_5	2	2	-1	-1	0	0
Γ_6	2	-2	-1	1	0	0

For $\phi = \frac{\pi}{3} : \chi = \frac{\sin(l+\frac{1}{2})\frac{\pi}{3}}{\sin\frac{\pi}{6}} =$ 1, 2, 1, and -1 for l = 0, 1, 2, and 3, respectively.

For $\phi = \frac{2\pi}{3} : \chi = \frac{\sin(l+\frac{1}{2})\frac{2\pi}{3}}{\sin\frac{\pi}{3}} =$ 1, 0, -1, and 1 for l = 0, 1, 2, and 3, respectively

For $\phi = \pi : \chi = \frac{\sin(l+\frac{1}{2})\pi}{\sin\frac{\pi}{2}} =$ 1, -1, 1, and -1 for l = 0, 1, 2, and 3, respectively

For $\phi = \frac{4\pi}{3} : \chi = \frac{\sin(l+\frac{1}{2})\frac{4\pi}{3}}{\sin\frac{2\pi}{3}} =$ 1, 0,-1, and 1 for l = 0, 1, 2, and 3, respectively

For $\phi = \frac{5\pi}{3} : \chi = \frac{\sin(l+\frac{1}{2})\frac{5\pi}{3}}{\sin\frac{5\pi}{6}} =$ 1, 1, 1, and -1 for l = 0, 1, 2, and 3, respectively

we obtain the following table

Table 10: Characters of classes of C_{6v} in the $(2l+1)$-dimensional representation D^l and the resolution of D^l into irreducible representation of C_{6v}

l	E	C_6^3	$C_6^2(2)$	$C_6(2)$	$\sigma_v(3)$	$\sigma_{v'}(3)$	
0	1	1	1	1	1	1	$D^0 = \Gamma_1$
1	3	-1	0	2	-1	-1	$D^1 = \Gamma_2 + \Gamma_5$
2	5	1	-1	1	1	1	$D^2 = \Gamma_1 + \Gamma_5 + \Gamma_6$
3	1	-1	1	-1	-1	-1	$D^3 = \Gamma_2 + \Gamma_3 + \Gamma_4 + \Gamma_5 + \Gamma_6$
4	9	1	0	-2	1	1	$D^4 = \Gamma_1 + \Gamma_3 + \Gamma_4 + \Gamma_5 + 2\Gamma_6$
5	11	-1	-1	-1	-1	-1	$D^5 = \Gamma_2 + \Gamma_3 + \Gamma_4 + 2\Gamma_5 + 2\Gamma_6$
6	13	1	1	1	1	1	$D^6 = 2\Gamma_1 + \Gamma_2 + \Gamma_3 + \Gamma_4 + 2\Gamma_5 + 2\Gamma_6$

Table 11: Double-Valued Representations of C_{6v}

C_{6v}	E	R	C_6^3 C_6^3R	C_6^4 C_6^2R	C_6 C_6^5R	C_6^2 C_6^4R	C_6^5 C_6R	$\sigma_v(3)$ $\sigma_vR(3)$	$\sigma_{v'}(3)$ $\sigma_{v'}R(3)$
Γ_7	2	-2	0	1	$\sqrt{3}$	-1	$-\sqrt{3}$	0	0
Γ_8	2	-2	0	1	$-\sqrt{3}$	-1	$\sqrt{3}$	0	0
Γ_9	2	-2	0	-2	0	2	0	0	0

For $\phi = 0 : \chi_1 = 2j+1, \chi_2 = -\chi_1$

For $\phi = \frac{\pi}{3} : \chi_3 = \frac{\sin(j+\frac{1}{2})\frac{\pi}{3}}{\sin\frac{\pi}{6}} = \sqrt{3}, 0$ for j = $(\frac{1}{2}, \frac{3}{2})$ and $\frac{5}{2}$, respectively.

For $\phi = \frac{2\pi}{3}, \chi_4 = \frac{\sin(j+\frac{1}{2})\frac{2\pi}{3}}{\sin\frac{\pi}{3}} =$ 1, -1, and 0 for $j = \frac{1}{2}, \frac{3}{2}$ and $\frac{5}{2}$, respectively.

For $\phi = \pi : \chi_5 = 0$

For $\phi = \frac{4\pi}{3} : \chi_6 = \frac{\sin(j+\frac{1}{2})\frac{4\pi}{3}}{\sin\frac{2\pi}{3}} =$ -1, 1, and 0 for j $= \frac{1}{2}, \frac{3}{2}, \frac{5}{2}$, respectively.

For $\phi = \frac{5\pi}{3} : \chi_7 = \frac{\sin(j+\frac{1}{2})\frac{5\pi}{3}}{\sin\frac{5\pi}{6}} = -\sqrt{3}, 0$ for $j = (\frac{1}{2}, \frac{3}{2})$ and j $= \frac{5}{2}$, respectively.

Finally, we obtain the table 12.

Table 12: Characters of C_6v in the $(2j+1)$-dimensional representation and the resolution of D^j into irreducible representations of C_{6v}

.

j	K_1	K_2	K_3	K_4	K_5	K_6	K_7	K_8	K_9	
$\frac{1}{2}$	2	-2	0	1	$\sqrt{3}$	-1	$-\sqrt{3}$	0	0	$D^{\frac{1}{2}} = \Gamma_7$
$\frac{3}{2}$	4	-4	0	-1	$\sqrt{3}$	1	$-\sqrt{3}$	0	0	$D^{\frac{3}{2}} = \Gamma_7 + \Gamma_9$
$\frac{5}{2}$	6	-6	0	0	0	0	0	0	0	$D^{\frac{5}{2}} = \Gamma_7 + \Gamma_8 + \Gamma_9$
$\frac{7}{2}$	8	-8	0	1	$-\sqrt{3}$	1	$\sqrt{3}$	0	0	$D^{\frac{9}{2}} = \Gamma_7 + 2\Gamma_8 + \Gamma_9$
$\frac{9}{2}$	10	-10	0	-1	$-\sqrt{3}$	1	$\sqrt{3}$	0	0	$D^{\frac{9}{2}} = \Gamma_7 + 2\Gamma_8 + 2\Gamma_9$
$\frac{11}{2}$	12	-12	0	0	0	0	0	0	0	$D^{\frac{11}{2}} = 2\Gamma_7 + 2\Gamma_8 + 2\Gamma_9$

Reducing the continuous angles $0 \subseteq \phi \subseteq 2\pi$ for full rotation groups (FRG), to the particular point group rotations $C_6(\phi = 0, \frac{\pi}{3}, \frac{2\pi}{3}, \frac{3\pi}{2}, \frac{4\pi}{2}, \frac{5\pi}{2})$, we have calculated the characters of $\chi^l(\phi)$ and $\chi^j(\phi)$ for given l and j. On the other hand, the point group C_6 has got its own irrps tabulated(CDML) (see tables 9 and 11). For l = 1 and $\phi : 0, \frac{\pi}{3}, \frac{2\pi}{3}, \frac{3\pi}{2}, \frac{4\pi}{2}, \frac{5\pi}{2})$, the matrix of D^l is one of 3×3 which is not in the set of irrps of C_6 group. It follows that $D^{l=1}(\phi)$ is one of the reducible representations of the C_6 group, with hexagonal base (x, y, z) shown in Fig.10.

For the orbital angular momentum l-integer, the spectral terms of an atom are classified according to single-value irreducible representations (SV irrps) $D^l(\alpha, \beta, \gamma$ - Euler angles) of the full rotation group of the atom, while for the total angular momentum j $= l \pm s$ (half integer: spin included) the states are classified according to the double-valued (DV) irreducible representations $D^j(\alpha\beta\gamma)$. The characters of the SV irrps (D^l) and DV irrps (D^j) of the 32 crystallographic point groups and 230 space groups are readily available in CDML tables.

The $D^{l=1}$ and $D^{l=2}$ representations etc... can be reduced into irrps of C_6 by means

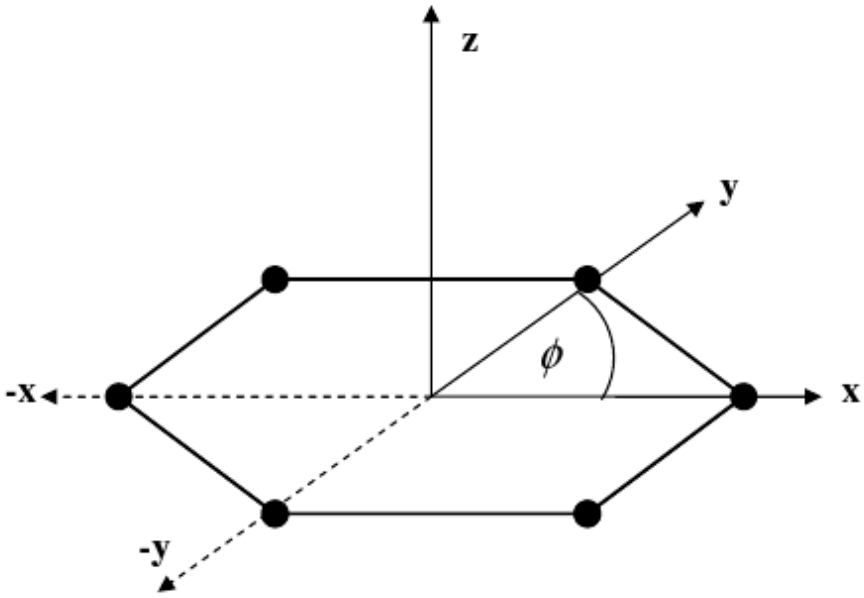

Figure 10: Hexagonal crystal basis

of the reduction formulas

$$a_\mu = \frac{1}{g}\sum_\mu g_i \chi_i^l(\phi)\chi_i^{(\mu)}(\phi) \tag{29}$$

$$a_\sigma = \frac{1}{g}\sum_\sigma g_i \chi_i^j(\phi)\chi_i^{(\sigma)}(\phi) \tag{30}$$

for l integer and j half-intenger, respectively.

The χ^l and χ^j stand for the characters of the full rotation group $(\alpha, \beta, \gamma\ )$ reduced in crystal to rotations of a point group ϕ, and χ^μ are characters of a point group of the crystalline field. $\mu \equiv \Gamma_1, \Gamma_2, ..., \Gamma_6$ and $\sigma \equiv \Gamma_7, \Gamma_8, \Gamma_9$.

The characters $\chi^l(\phi)$ while $\chi^j(\phi)$ are listed in tables 9 and 11 with the characters of Γ_i (i = 1 - 6) and Γ_k (k = 7 - 9) tabulated in tables 8 and 10.

Using the reduction formulas Eq. 29 and 30, we determined the splittings of the spectral terms of free atoms and for greater understanding we have shown and derived that if the free atoms placed in the ZnO crystal, the levels split into new terms belonging to the irreducible representations of the crystal group (C_{6V}) see tables 10 and 12.

Consider $l = 1$ and $\mu = \Gamma_1$ and Γ_6.

From the reduction formula we have:

For $= \mu = \Gamma_2 : \frac{1}{12}[(3 \times 1) + (-1 \times 1) + 2(0 \times 1) + 2(2 \times 1) + 3(-1 \times -1) + 3(-1 \times -1)] = 1$

For $= \mu = \Gamma_6 : \frac{1}{12}[(3 \times 2) + (-1 \times -2) + 2(0 \times -1) + 2(2 \times 1) + 3(-1 \times 0) + 3(-1 \times 0)] = 1$

We conclude that $D^1 = \Gamma_1 + \Gamma_6$: The p- state splits into Γ_1 and Γ_6 belonging to SV irrps of C_6v.

Consider l = 2 and $\mu = \Gamma_1, \Gamma_5$ and Γ_6.

For $\mu = \Gamma_1 : \frac{1}{12}[(5 \times 1) + (1 \times 1) + 2(-1 \times 1) + 2(1 \times 1) + 3(1 \times 0) + 3(1 \times 1)] = 1$

For $\mu = \Gamma_5 : \frac{1}{12}[(5 \times 2) + (1 \times 2) + 2(-1 \times -1) + 2(1 \times -1) + 3(1 \times 0) + 3(1 \times 0] = 1$

For $\mu = \Gamma_6 \frac{1}{12}[(5 \times 2) + (1 \times -2) + 2(-1 \times -1) + 2(1 \times 1) + 3(1 \times 0) + 3(\times 0)] = 1$

We conclude that $D^2 = \Gamma_1 + \Gamma_5 + \Gamma_6$: The d- state splits into Γ_1, Γ_5 and Γ_6 belonging to SV irrps of C_6v.

Consider $j = \frac{1}{2}$ and $\mu = \Gamma_7$

The reduction formula gives:

For $\mu = \Gamma_7 : \frac{1}{24}[(2 \times 2) + (-2 \times -2) + 2(0 \times 0) +$

$2(\sqrt{3} \times \sqrt{3}) + 2(-1 \times -1) + 2(-\sqrt{3} \times -\sqrt{3})] = 1$

$D^{\frac{1}{2}} = \Gamma_7$; the s-state doesn't split.

consider $j = \frac{3}{2}$ **and** $\mu = \Gamma_7$ **and** Γ_9

For $\mu = \Gamma_7$:

$\frac{1}{24}[(4 \times 2) + (-4 \times -2) + 2(0 \times 0) + 2(-1 \times 1) + 2(\sqrt{3} \times \sqrt{3}) +$

$2(1 \times -1) + 2(-\sqrt{3} \times -\sqrt{3}) + 6(0 \times 0) + 6(0 \times 0)] = 1$

For $\mu = \Gamma_9$:

$\frac{1}{24}[(4 \times 2) + (-4 \times -2) + 2(0 \times 0) + 2(-1 \times -2) + 2(\sqrt{3} \times 0) + 2(1 \times 2) +$

$2(-\sqrt{3} \times 0) + 6(0 \times 0) + 6(0 \times 0)] = 1$

The j = $\frac{3}{2}$ level splits into Γ_7 and Γ_9 symmetries of C_{6v}. $D^{\frac{3}{2}} = \Gamma_7 + \Gamma_9$

More results regarding the splitting of atomic levels when an atom is placed in the ZnO crystal are tabulated in tables 10 and 12.

3 Band structure of wurtzite ZnO at k = o and selection rules for optical transitions in the absence and presence of Time Reversal Symmetry.

3.1 Introduction

The lattice structure of ZnO belongs to the hexagonal system (space group C_{6V}^4). Based on its thermal, electric and opto-electronic properties ZnO is a material with enormous present applications. One device with promising commercial potential is a UV light-emitting diode (LED) which could be combined with phosphors to produce solid-state lighting. Another is a transparent field effect transitors, which could serve as an active element in large-area displays. The free exciton in ZnO has a binding energy of about 60meV; thus efficient excitonic emission processes can persist in ZnO at room temperature and higher [8]. furthermore bound excitons exhibit large binding energy. Particularly excitons bound to shallow donors: Al, Ga, and In give rise to the sharp transition peaks which can be useful in UV light-emitting diode devices. All these excitonic transitions originate at the $\mathbf{k = 0}$ centre of the Brillouin zone where the band structure is described by DV irrps. Therefore we will discuss the electronic band structure of ZnO in the next section.

3.2 Band structure of the wurtzite ZnO at $\mathbf{k = 0}$

ZnO is a wide direct band gap semiconductor ($E_g \sim 3.3eV$).
The band stracture of wurtzite compounds has been investigated by many authors[9]. However the effect of time reversal symmetry has not been considered.
Disregarding the spin-orbit (S-O) interaction, crystalline field (CF) and TRs effect, the free electrons occupy S-like conduction band (CB) states and free holes P (P_x, P_y, P_z) valence band (VB) states. The S-like states transform according to an irreducible representation (irrp) Γ_1^c of the C_{6v}- ZnO point group, while the P (P_x, P_y, P_z) hydrogenic like orbitals transform like X, Y, Z, according to the so-called vector representation V(x, y, z) [10]
The crystalline field splits the P_x, P_y, P_z states into $P_x, P_y(\Gamma_5(x, y))$ and $P_z(\Gamma_1(z))$ states. The vector representation for ZnO is reducible to Γ_1 and Γ_5 irrps $V = \Gamma_1(z)+\Gamma_5(x, z)$. The inclusion of S-O interaction results in further splittings : $\Gamma_1^c \otimes D_{\frac{1}{2}} = \Gamma_7^c$; $\Gamma_5^v \otimes D_{\frac{1}{2}} = \Gamma_7^v + \Gamma_9^v$

and $\Gamma_1^v \otimes D_{\frac{1}{2}} = \Gamma_7^v$ (see Fig.14). This yields the historically established valence band ordering : $\Gamma_9^v(A)\,\Gamma_7^v(B)\,\Gamma_7^v(C)$, where the letters A, B, and C label the three different types of excitons respectively (see Fig.11 and 12)[11].

The free electrons in the conduction band (CB) and holes in the valence bands (VBs) are classified according to double-valued irrps.

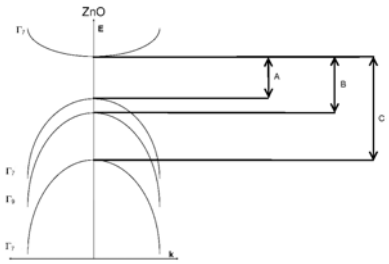

Figure 11: Band structure and symmetry of hexagonal ZnO in case of $\Gamma_7^v(A)\,\Gamma_9^v(B)\,\Gamma_7^v(C)$ valence band ordering

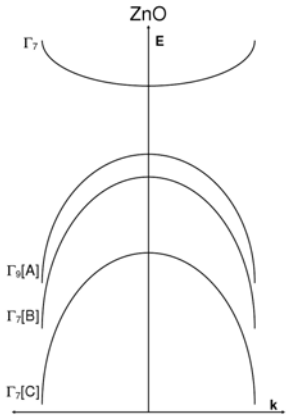

Figure 12: Band structure and symmetry of hexagonal ZnO in case of $\Gamma_9^v(A)\,\Gamma_7^v(B)\,\Gamma_7^v(C)$ valence band ordering

3.3 The effect of TRS on band structure and classification of states

Replacing t by -t and taking the complex conjugate of any time-dependent Schrödinger equation, we obtain $\psi_{\mathbf{i}}^{\star}(\tilde{\mathbf{r}}, \mathbf{t})$ wave functions which are also an eigenfunctions of $\hat{H}_{sch}$ together with the $\psi_{\mathbf{i}}(\tilde{\mathbf{r}}, \mathbf{t})$. The ψ_i are the basis of the D irrp of the group of $\hat{H}_{sch}$ while $\psi^{\star}$ are the basis of $D^{\star}$. When D and $D^{\star}$ are complex the state of a system (energy term) will be classified by the joint $D \oplus D^{\star}$ irrps. Clearly, the degeneracy of a state increases twice. In order to determine whether or not the TRS is present in a system, one must to to find all complex irrps of a symmetry group of a Hamiltonian. Froöbenius and Schur [12] showed that it is sufficient to know only the characters of irrps in order to determine whether a representation is real or complex. The characters of 32 crystallographic point groups and 230 space groups are readily available in CDML tables [13]. I have tested all the irrps all irrps of the C_{6v} group. The following irrps are TRS degenerate:
Single-valued irrps for classification of spinless particle states (like phonons):$A_{1,2,3,4,5,6}, \Delta_{1,2,3,4,5,6}, H_{1,2}$, $L_{1,2,3,4}, U_{1,2,3,4}, P_{1,2,3}$ and $S_{1,2}$ of high symmetry points.
Double-valued irrps for particles with $S = \frac{1}{2}, \frac{3}{2}$...(spinors): $\Gamma_{6,7,8}$ of point and space groups. The double-valued irrps of 32 crystallographic point groups and 230 space groups are normally complex and therefore TR degenerated. Consequently, the states of free electrons and holes at $\ddot{\mathrm{K}} = 0$ in ZnO are supposed to be classified by joint irrps $\Gamma_7^c \oplus (\Gamma_7^c)^{\star}, \Gamma_9^v \oplus (\Gamma_9^v)^{\star}$ and $\Gamma_7^v \oplus (\Gamma_7^v)^{\star}$. Fig.14 displays the effect of TRS on the band structure.

3.4 Selection rules for optical transitions in wurtzite structure in the absence of TRS

In the absence of accidental degeneracy and TRS, the matrix elements of a perturbation $\hat{f}$ between the conduction CB and VB states take the form $\int(\Psi_i^c)^* \hat{f} \varphi_j^v d\vec{r}$, which is non-zero when the corresponding Kronecker product $\Gamma^c \otimes D^f \otimes \Gamma^v$ contains the unit representation normally denoted as Γ_1 or A_1[13]. The D^f is a representation (not necessarily irreducible) according to which the perturbation operator transforms. In the case of absorption (emission) of electromagnetic radiation, the dipole moment operator: $\hat{f} = \hat{d}$ for the electric dipole radiation transforms like X, Y, Z (vector rep $V = \Gamma_1(z) + \Gamma_5(x, y)$) in ZnO.

For $\tilde{\mathbf{E}} \parallel \mathbf{c}$ (c-hexagonal axis along Z) the SR_s are: $\Gamma_7^c \otimes \Gamma_1(z) \otimes \Gamma_7^v = \Gamma_1 + \Gamma_2 + \Gamma_5$ (allowed transitions for A-and C-excitons) and $\Gamma_7^c \otimes \Gamma_1(z) \otimes \Gamma_9^v = \Gamma_5 + \Gamma_6$ (B-excitons, forbidden transition since the Kronecker product does not contain Γ_1 rep).
For $\tilde{\mathbf{E}} \perp \mathbf{c}$, we have : $\Gamma_7^c \otimes \Gamma_5(x, y) \otimes \Gamma_7^v = \Gamma_1 + \Gamma_2 + 2\Gamma_5 + \Gamma_6$ and $\Gamma_7^c \otimes \Gamma_5(x, y) \otimes \Gamma_9^v = \Gamma_1 + \Gamma_2 + \Gamma_6 + \Gamma_3 + \Gamma_4 + \Gamma_5$. For $\tilde{\mathbf{E}} \perp \mathbf{c}$ polarisation all transitions for A-, B-, C-excitons are allowed and observed experimentally [14].

3.5 Optical selection rules in the presence of TRS

As mentioned the electron and hole states are TR degenerated and therefore their states are classified according to the joint reps: $D \oplus D^{\star}$. Consequently, the respective selection rules are: For $\tilde{\mathbf{E}} \parallel \mathbf{c}$: $(\Gamma_7^c \oplus (\Gamma_7^c)^*) \otimes \Gamma_1(z) \otimes (\Gamma_9^v \oplus (\Gamma_9^v))^*)$. The decomposition of the KPs reveals $4\Gamma_5$ and $4\Gamma_6$ states. All the states have a different basis for functions and those can be obtained by Clebsch-Gordon Coefficients methods. The B-excitons are still forbidden as in the absence of TRS.

For $\tilde{\mathbf{E}} \parallel \mathbf{c}$:

$(\Gamma_7^c \oplus (\Gamma_7^c)^*) \otimes \Gamma_1(z) \otimes (\Gamma_7^v \oplus (\Gamma_7^v)^*) = 4\Gamma_1 + 4\Gamma_2 + 4\Gamma_5$. The transitions are also allowed as in the absence of TRS.

For $\tilde{\mathbf{E}} \perp \mathbf{c}$:

$(\Gamma_7^c \oplus (\Gamma_7^c)^*) \otimes \Gamma_5(x,y) \otimes (\Gamma_9^v + (\Gamma_9^v)^*) = (\Gamma_5 + \Gamma_6) \otimes \Gamma_5 + \ldots$ The transition is allowed for a B-exciton, since $\Gamma_1 \in$ in KP $\Gamma_5 \otimes \Gamma_5$

For $\tilde{\mathbf{E}} \perp \mathbf{c}$:

$(\Gamma_7^c \oplus (\Gamma_7^c)^*) \otimes \Gamma_5(x,y) \otimes (\Gamma_7^v + \Gamma_7^v) = 4(\Gamma_1 + \Gamma_2 + \Gamma_3 + \Gamma_4 + \Gamma_5 + \Gamma_6)$. Again these transitions are allowed.

Clearly the TRS does not change the existing SRs introducing only a number of new states of the same symmetry Fig.13 All the states are based on different wave functions, which correspond to different energy levels. Further splitting due to TRS is possible. The effect of TRS on phonons and TR splitting has been experimentally observed[15]. Recent studies of the electronic band structure of ZnO, by means of first-principles calculations and density-functional theory clearly evidence the existence of TRS on high symmetry point A and Δ line in ZnO and other wurtzite compounds.

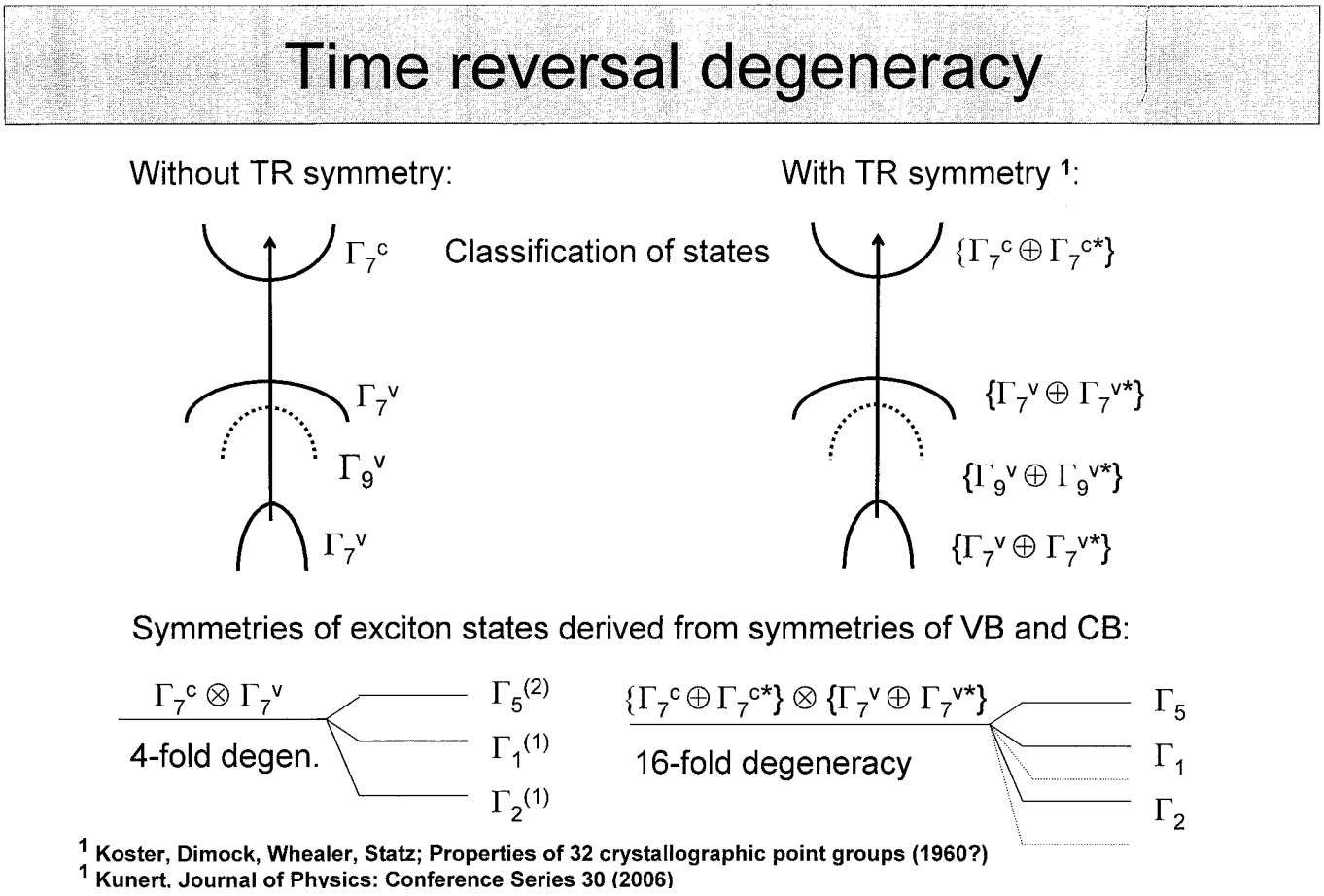

Figure 13: Time Reversal degeneracy

4 Experimental results and discussions

4.1 Introduction

When crystals are excited by laser or other radiation, electrons are removed from the valence band, and placed in the conduction band leaving holes in the valence band. Because of the mutual attraction between the electrons and holes, these particles can exist as pairs or excitons which can move throughtout the crystal. The excitons can be trapped at donors or acceptors in either neutral or ionized states or can be localized in such a way that the electron-hole recombination processes produce an emission spectrum with many different components. The purpose of this section is to introduce the interpretation of the spectra.

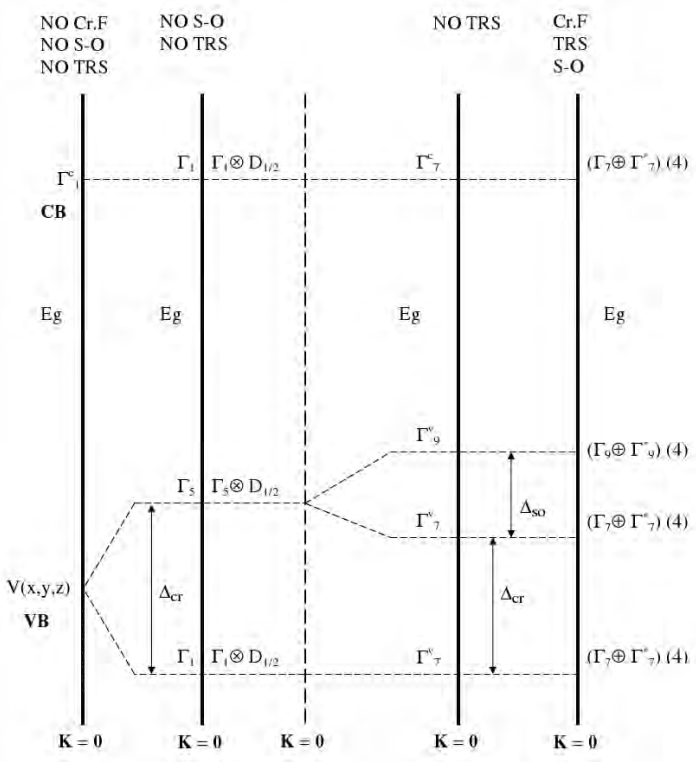

Figure 14: Band structure and selection rules for wurtzite compounds at the Γ symmetry point ($\mathbf{k} = \mathbf{0}$). The V stands for 3×3 dimensional vector representation which is reducible to $\Gamma_1(z) + \Gamma_5(x, y)$. There are a number of wurtzite compounds for which the above band structure is valid. In some of them the crystalline field is rather negligeable. For them the very first left diagram of band structure may be relevant. Our figure can be directly compared with figure 1 in [16]. Birman assigned the top valence band of ZB structure to Γ_4 rep. The Γ_4 rep is one of the irrps of the ZB space group and it is simultaneously a vector representation of the group. For wurtzite, similar assignment on Birman's figure is missing

.

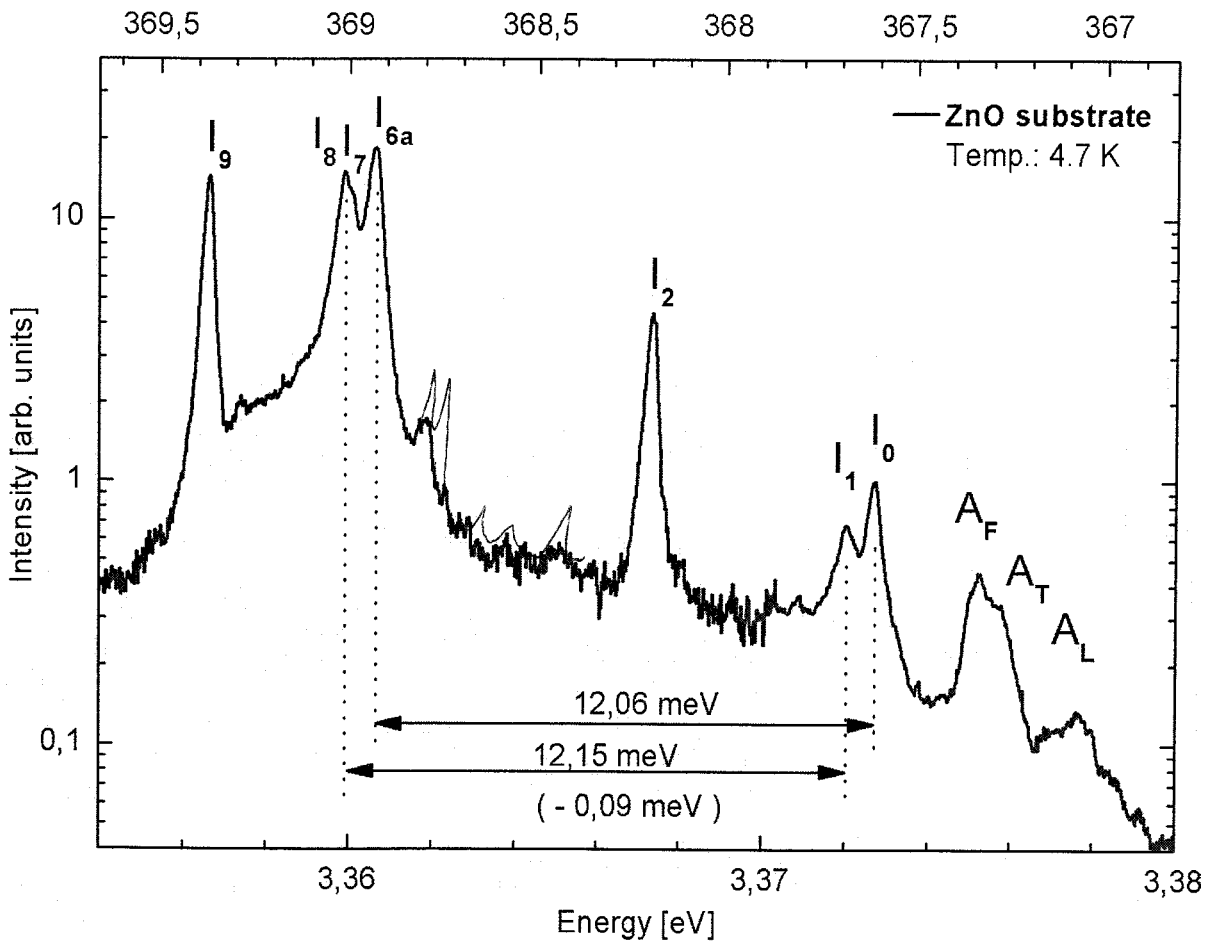

Figure 15: Free and bound excitons: Free excitons (A_T, A_L), ionised donor (I_0, I_1 and I_2) and neutral donor (I_{6a}, I_7, I_8 and I_9)

4.2 Photoluminescence from ZnO

Photoluminescence (PL) is a technique which is used to investigate the extrinsic optical properties of a material. It is a process in which a substance absorbs photons and then re-radiates photons. Quantum mechanically, this can be described as an excitation to a higher energy state accompanied by the emission of a photon. This is one of many forms of luminescence (light emission) and is distinguished by photoexcitation (excitation by photon).

If the material is irradiated with electromagnetic radiation, the resultant emission is termed photoluminescence. Luminescence excited by bombardment by the energetic electrons is termed cathodoluminescence.

X-ray luminescence follows irradiation by X-rays.

Chemiluminescence follows excitation by chemical reactions. Electroluminescence is luminescence excited by applying a voltage to the materials.

There are several advantages of PL such as: it is possible to determine the band gap, any impurities and defects in the materials, recombination mechanisms and quality of material.

- **Experimental Procedure**

Lithium doped ZnO epilayers were grown by chemical vapour deposition on ZnO substrates. Photoluminescence (PL) and Magneto-photoluminescence (MPL) measurements were performed using a 325nm HeCd laser. Fig.16 displays the photoluminescence at 4.2 Kelvin in the energetic range of the free and bound excitons.

The most prominent excitonic transition lines are the I_9 (3.3567 eV), I_8(3.3598 eV), I_{6a}(3.3604 eV), I_2(3.3674 eV), I_1(3.3718 eV), and I_0(3.3726 eV).

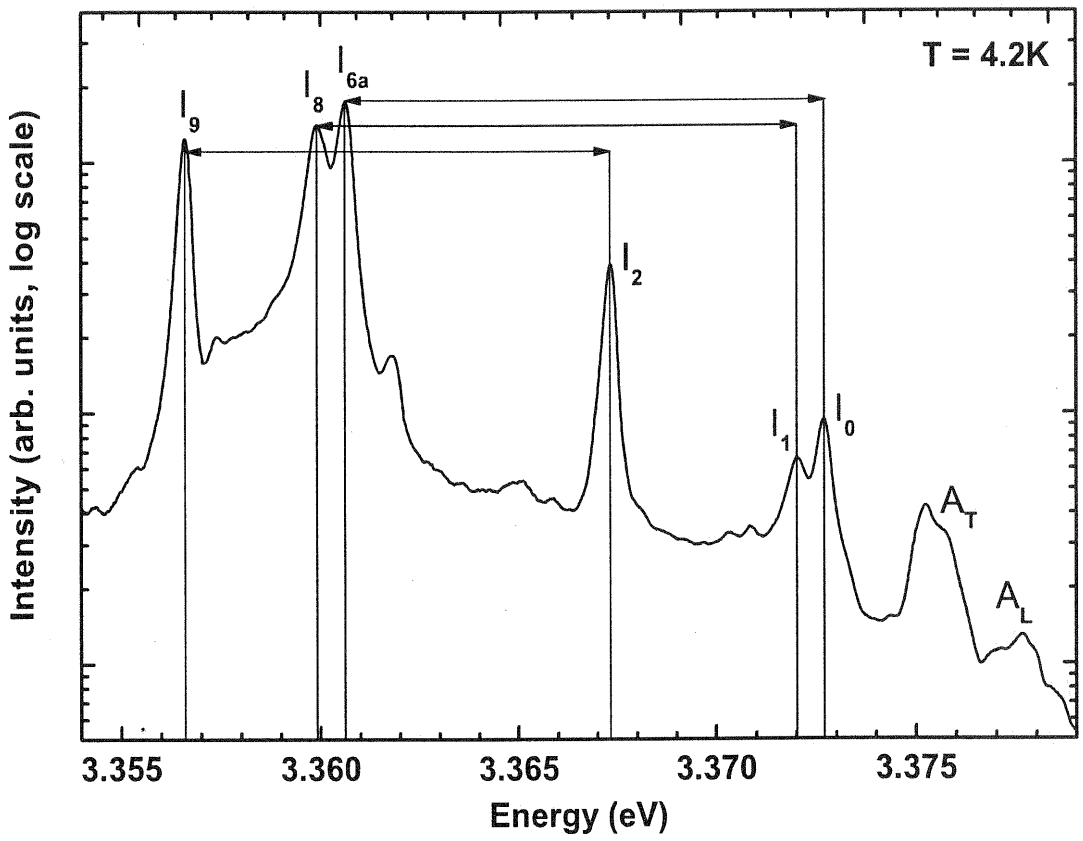

Figure 16: PL spectra of lithium doped high quality ZnO grown by CVD at a temperature of 4.2 Kelvin.

Table 13: Symbols in common use for labelling recombination processes

Free exciton	X	+-
Donor	D^0	$\oplus$ -
Acceptor	A^0	$\ominus$ +
Exciton bound at neutral donor	D^0, X	$\oplus = +$
Exciton bound at ionized donor	D^+,X	$\oplus$ - +
Exciton bound at neutral acceptor	A^0,X	$\ominus$ ++ -
Exciton bound at ionized acceptor	A^-,X	$\ominus$ + -
Free electron to acceptor	e,A^0	
Donor to free hole	D^0,h	

Previous studies have shown that I_9, I_8 and I_{6a} are neutral exciton complexes bound to an indium [17], gallium [18] and aluminium [19] impurity, respectively. These lines are accompanied by the higher lines I_0, I_1 and I_2. The neutral bound exciton line I_9 is correlated to I_2, I_8 to I_1 and I_{6a} to I_0. In fact, all investigated samples exhibit only I_0 to I_2 excitons if the related excitons I_{6a} to I_9 are present as well. Due to a similar scaling in intensity and energetic position, it is likely that these correlated pairs of transition lines are excitons bound to an impurity of the same chemical identity but in a different charge state.

Consequently, we attribute I_0, I_1 and I_2 to ionized donor bound related to Al, Ga and In impurities, respectively. Concerning the I_1 complex, this correlation is in agreement with data published by Johnston et al. [18]., who reported a simultaneous decrease of the I_8 and I_1 intensity for ZnO crystals doped with a radioactive Ga isotope.

The various bound exciton complexes with their localisation energies and suggested chemical identities are summarized in table14.

Table 14: Bound exciton complexes in ZnO. Energetic positions are given for T = 4.2 Kelvin

Line	$E(eV)$	$E_b(eV)$	Complex	Chem. element
I_9	3.3567	19.2	D^0X	In
I_8	3.3598	16.1	D^0X	Ga
I_{6a}	3.3604	15.5	D^0X	Al
I_2	3.3674	8.5	D^+X	In
I_1	3.3718	4.1	D^+X	Ga
I_0	3.3726	3.3	D^+X	Al

4.3 Magnetophotoluminescence from ZnO

The charge states of the bound exciton complexes are investigated by magneto-photoluminescence spectroscopy. Excitons bound to ionized impurities can be distinguished from those bound to neutral impurities by a nonlinear splitting of energy levels in the magnetic field perpendicular to the c axis of the crystal, while excitons bound to neutral impurities exhibit a linear splitting behaviour for $\vec{B} \perp c$ [20] Fig.17.
Futhermore, an additional low energy transition due to zerofield splitting appears for I_0 and I_1 if a magnetic field is applied. Such an interaction can not occur in transitions originating from excitons bound to neutral impurities, since the spin of the two equal particles are anti-parallel.

For ionized bound excitons at low magnetic fields, only a high energy Zeeman component, resulting from a Γ_5 state is visible, whereas the low energy component, originating from Γ_1 to Γ_6, transition is forbidden by selection rules. However, for larger magnetic fields, the selection rules can be relaxed due to a spin-spin interaction of Γ_5 states with anti-parallel spin, mixed with Γ_6 states with parallel spin, thus allowing the appearance of a new line associated with the Γ_6.

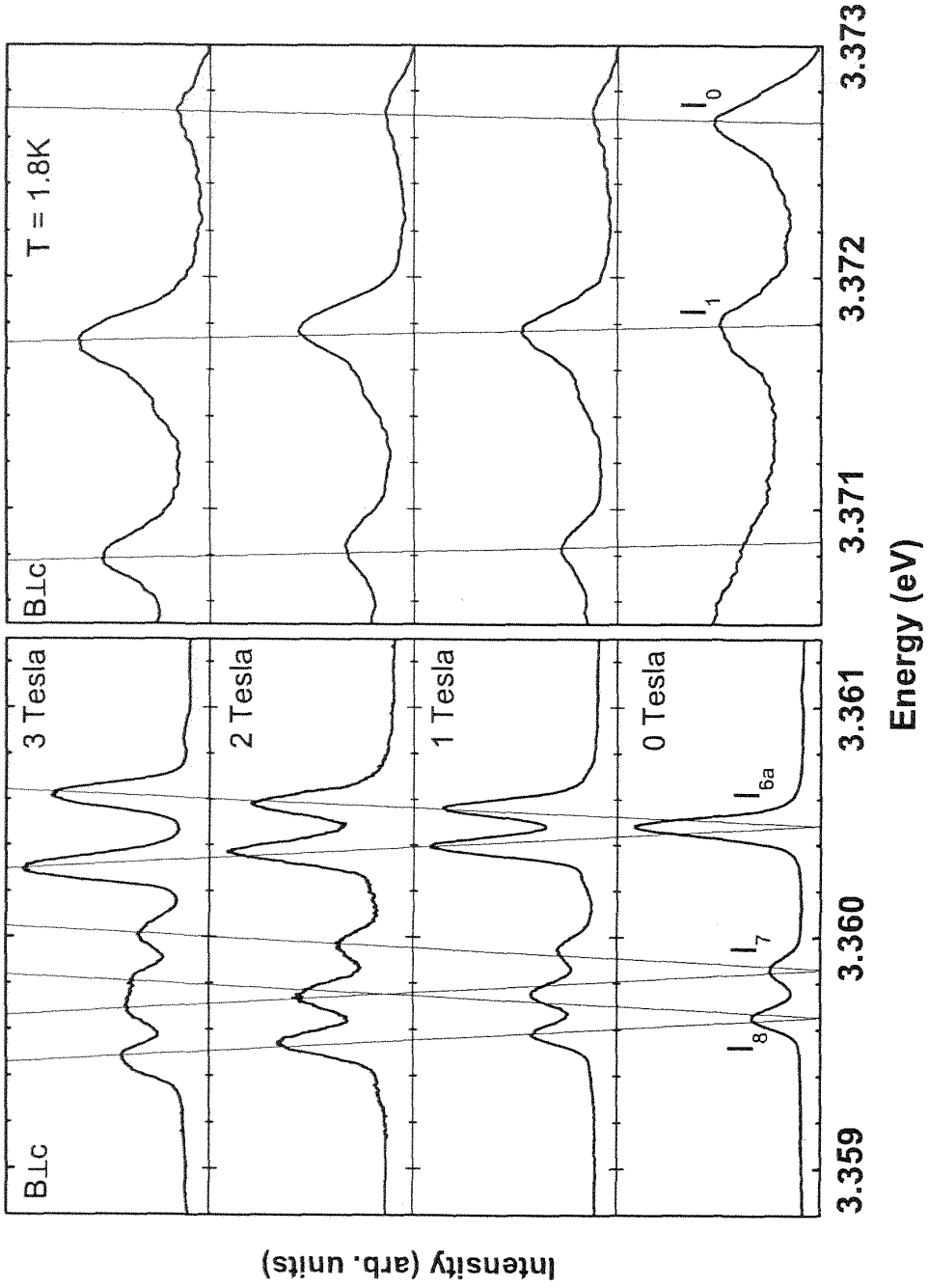

Figure 17: Zeeman splitting of neutral and ionized donor bound excitons for magnetic fields of 0-3 Tesla. Spectra are taken at 1.8 Kelvin in Voigt geometry ($\vec{B} \perp c$).

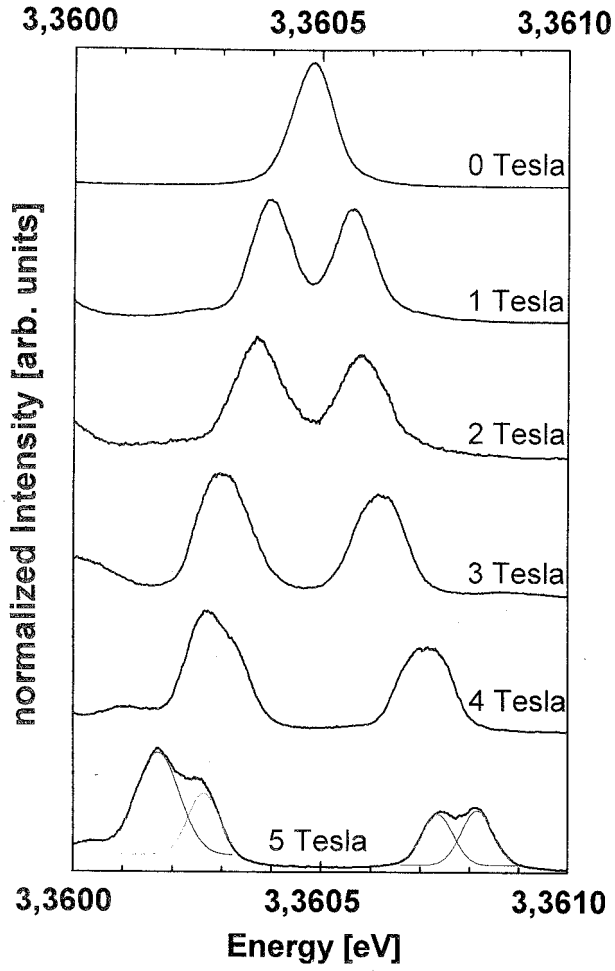

Figure 18: PL: I_{6a} Zeeman splitting

The extrapolation of the peaks positions to B = 0 Tesla reveals the presence of zerofield splitting, ascribed to spin-spin interaction energy Fig.18

.

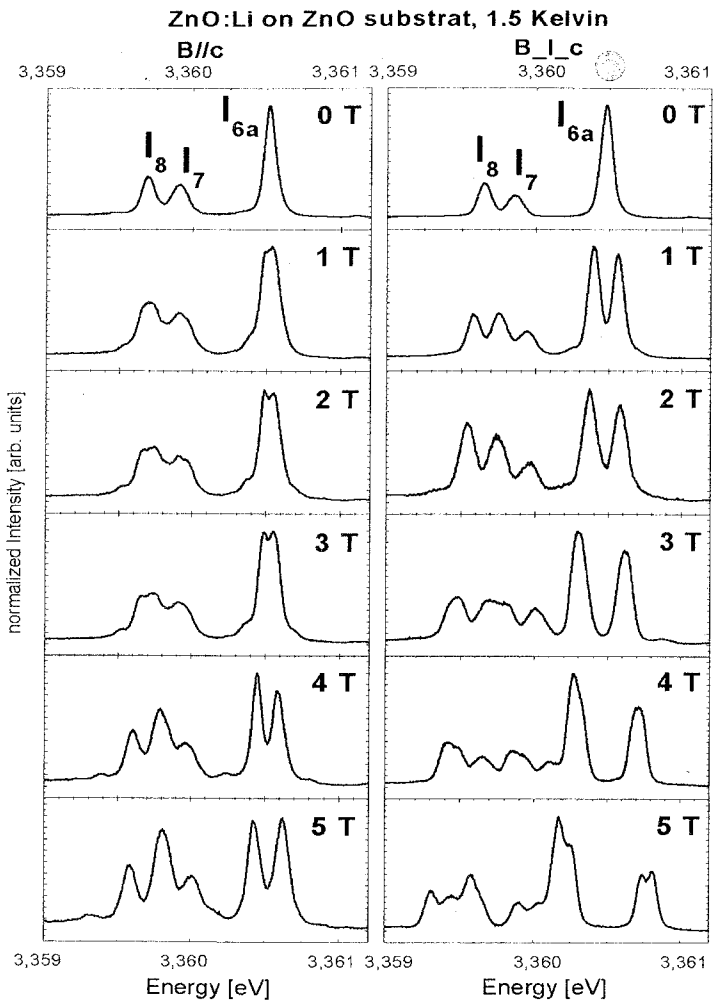

Figure 19: Zeeman splitting I_8, I_7 and I_{6a} bounds excitons in $B \parallel$ C and $B \perp c$

As we introduced before, the atomic ground states of the elements listed in table 2 are Li(n =2 $^2S_{\frac{1}{2}}$), Al(n = 3 $^2P_{\frac{1}{2}}$), Ga (n = 4 $^2P_{\frac{1}{2}}$) and In (n = 5 $^2P_{\frac{1}{2}}$), where n is the principal quantum number. These states are doublets (2s+1 =2) and therefore exhibit anomalous Zeeman splitting. In ZnO, these dopants become shallow donors to which the excitons of symmetries $\Gamma_7^c \oplus \Gamma_7^v$ (A), $\Gamma_7^c \oplus \Gamma_9^v$(B) and $\Gamma_7^c \oplus \Gamma_7^v$(C) are bound. The excitons bound to the dopants states do not contribute to the spin states of complexes. These complexes remain doublets. Consequently, it follows that, the band I_{6a} (and others up to I_9) originates from the complexes (neutral donor excitons) of the total spin $S = \frac{1}{2}$. These are doublets $(S = \frac{1}{2}, 2S + 1 = 2)$, $m_s = \frac{-1}{2}, \frac{1}{2}$ (Fig19).

5 Conclusion

ZnO exhibits a strong potential for various short-wavelength optoelectronic device applications. In order to attain the potential offered by ZnO, both high-quality n-and p-type ZnO are indispensable. The ZnO with a wurtzite structure is naturally an n-type semiconductor because of a deviation from stoichiometry due to the presence of intrinsic defects such as O vacancies and Zn interstitials.

Undoped ZnO shows intrinsic n-type conductivity with very high electron densities of about $10^{21} cm^{-3}$.

The bound exciton complexes are observed as sharp-line optical transitions in photoluminescence (PL). I_9 is correlated to I_2, I_8 to I_1, and I_6a to I_0. While I_9, I_8, I_6a, are neutral exciton complexes bound to an In, Ga and Al impurity, respectively and I_0, I_1 and I_2 are ionized donor bound excitons related to Al, Ga and In, respectively (see fig 16).

The existence of a correlation between ionized and neutral bound excitons has been demonstrated.

The inclusion of extra degeneracy due to TRS reveals a number of new states of the same symmetries and essentially does not change the existing optical selection rules.

The selection rules discussed are related to absorption (emission) transitions observed by reflectivity measurements [21, 22]. Using the selection rules we have investigated allowed transitions between the conduction and valence bands.

References

[1] A. Enge Harald, M. Russel Wehr, James A. Richards; *Introduction to atomic physics*, Addison-Wesley, (1973).

[2] H. Haken; *Atomic and quantum physics: An introduction to the fundamentals of experiment and theory*, New York; Springer-Verlag (1987).

[3] V.A.Karasyuk, D. G. S. Beckett, M. K. Nissen, A. Villemaire, T.W.Steiner,and M. L. W. Thewalt; Phys. Rev B **49** (1994), 23.

[4] B. Lax, L.M.Roth and S. Zwerdling; J. Phys. Chem. Solids **8** (1958), 311-318.

[5] Harvey Elliot White; *Introduction to atomic spectra*, M_c Graw-Hill, (1934).

[6] Morton Hamermesh; *Group theory and its application to physical problems*, Addison-Wesley, (1962).

[7] Michael Tinkham; *Group theory and quantum mechanics*, McGraw-Hill (1964).

[8] *Ü. Özgür*, Ya. I. Alivov , C.Liu, A. Reshchikov, S. Dogan, V. Avrutin, S.-J. Cho, and H. Morkoc; *Journal of Applied Physics*, **98** ,(2005), 041301.

[9] W.R.L. Lambrecht, A.V Rodina, S. Limpijumnong, B.Segall, and B.K Meyer, Phys.Rev. B 65, 075207 (2002).

[10] M. R. Wagner, H.W. Kunert, A. G. J. Machatine, P. Niyongabo, A. Hoffiman, J. Malherbe, and J. Barnas; *Bound and free Excitons in ZnO. Optical selection rules in the absence and presence of Time Reversal Symmetry* (2008).

[11] B. K. Meyer et al.; Phys. stat. sol. **241**, (2004).

[12] G. Fröbenius and I. Schur, Berl. Ber.186 (1906).

[13] A. P. Cracknell, B.L. Davis, S. C. Miller, and W.F.Love; Kronecker Product Tables Vol 4 (IFI/Plenum Press, New York, Washington, London,(1979)).

[14] Y. S. Park, C .W. Litton, T. C. Collins, and D. C. Reynolds, Phys. Rev. **143**, (1966), 512.

[15] D.C. Thomas and J.J. Hopfield, Phys. Rev. 128,2135 (1962).

[16] Y. S. Park, C. W. Litton, T. C. Collins, and D. C. Reynolds; Physical Review, **143**, (1966), 2.

[17] S. Müller, D. Stichtenoth, M. Uhrmacher, H. Hofsäss, C. Ronning, and J. Röder Appl. Phys. Lett. **90** (2007), 012107.

[18] K. Johnston, M.O. Henry, D. McCabe, E. McGlynn, M. Dietrich, E. Alves, and M. Xi, Phys. Rev. B **73** (2006), 165212.

[19] B. K. Meyer, J. Sann, S. Lautenschläger, M. R. Wagner, and Hoffmann, Phys. Rev. B **76** (2007) 184120

[20] K. Thoma, B. Dorner, G. Duesing , and W. Wegener; Sol. Stat. Comm. **12**(1974) 11111.

[21] D. G. Thomas and J. J. Hopfield, Phys. Rev. Lett.**7** (1961) 316.

[22] A. W. Hewat; Sol. Stat. Comm. **8** (1974), 187.

Appendix

1. **Determination of the frequencies of the electronS oscillating in a magnetic field: Normal Zeeman effect**

In the absence of any external perturbation like a steady state magnetic $\bar{B}$, and electric field $\bar{E}$ or alternate laser light $\vec{E} = \vec{E_0}e^{-i(k\vec{r}-\omega t)}$ and others the equation of an electron is

$$m_e\frac{d\vec{v}}{dt} = -m_e\omega_0^2\vec{r} - e\vec{v}\times\vec{B}. \tag{31}$$

$$\vec{r} = \vec{r_0}e^{-i\omega_0 t} \tag{32}$$

It follows that the electron trajectory along the axis x, y, and z oscillates with the frequency ω_0. Applying a steady state magnetic field along the z axis we have

$B_z = B \neq 0$ and $B_x = B_y = 0$

$$\vec{r}\times\vec{B} = \begin{pmatrix} \vec{i} & \vec{j} & k \\ x & y & z \\ 0 & 0 & B \end{pmatrix} = \vec{i}(yB) - \vec{j}(xB)$$

$$\omega_0^2\left(\vec{i}x + \vec{j}y + \vec{k}z\right) = i\tfrac{e}{m_e}\omega\left(\vec{i}yB - \vec{j}xB + \vec{k}.0\right) + \omega^2\left(x\vec{i} + y\vec{j} + z\vec{k}\right)$$

$$\omega_0^2 x = 2i\tfrac{eB}{2m_e}\omega y + \omega^2 x$$

$$\omega_0^2 y = -2i\tfrac{eB}{2m_e}\omega x + \omega^2 y$$

$$\omega_0^2 z = \omega^2 z.$$

substituting $\frac{eB}{2m_e} = \Omega_L$ we obtain:

$$\omega_0^2 x - 2i\omega\Omega_L y - 0z = \omega^2 x$$

$$2i\omega\Omega_L x + \omega_0^2 y + 0z = \omega^2 y$$

$$\omega_0^2 z = \omega^2 z$$

$$\begin{pmatrix} \omega_0^2 & -2i\omega\Omega_L & 0 \\ 2i\omega\Omega_L & \omega_0^2 & 0 \\ 0 & 0 & \omega_0^2 \end{pmatrix}\begin{pmatrix} x \\ y \\ z \end{pmatrix} = \omega^2\begin{pmatrix} x \\ y \\ z \end{pmatrix} \tag{33}$$

$$\begin{vmatrix} \omega_0^2 - \omega^2 & -2i\omega\Omega_L & 0 \\ 2i\omega\Omega_L & \omega_0^2 - \omega^2 & 0 \\ 0 & 0 & \omega_0^2 - \omega^2 \end{vmatrix} = 0 \tag{34}$$

This gives :

$$\left\{\omega^4 - \left(2\omega_0^2 - 4\Omega_L^2\right)\omega^2 + \omega_0^4\right\}\left(\omega^2 - \omega_0^2\right) = 0$$

$$\omega^4 - \left(2\omega_0^2 + 4\Omega_L^2\right)\omega^2 + \omega_0^4 = 0$$

$(\omega^4 - 2\omega_0^2\omega^2 + \omega_0^4) - 4\Omega_L^2\omega^2 = 0$

Taking : $\omega^2 = p$ we get

$p^2 - (2\omega_0^2 + 4\Omega_L^2)\, p + \omega_0^4 = 0$; generally we have

$ap^2 + bp + c = 0$ with a = 1, b = $-(2\omega_0^2 + 4\Omega_L^2)$ and c = ω_0^4

The solution of the above equation yields the frequencies of an oscillating electron in a magnetic field **B**.

$p_{1/2} = \frac{-b \pm \sqrt{\Delta}}{2a}$ with $\Delta = b^2 - 4ac$

$\sqrt{\Delta} = \pm 4\Omega_L \sqrt{\Omega_L^2 + \omega_0^2}$

But: $\Omega_L \subset\subset \omega_0$

Therefore $\sqrt{\Delta} = \pm 4\Omega_L\omega_0$

$(\omega^2)_{1/2} = \omega_0^2 + 2\Omega_L^2 \pm 4\Omega_L\omega_0$

Dropping 2 in: $2\Omega_L^2$ because : $\Omega_L \subset\subset \omega_0$ we have : $(\omega^2)_{1/2} = (\omega_0 \pm 2\Omega_L)^2$. Finally we obtain: $\omega \cong \omega_0 \pm \Omega_L$. Substituting $\omega \cong \omega_0 \pm \Omega_L$ into Eq 34 we have:

$$r = \begin{pmatrix} cos(\omega_o - \Omega_L)t \\ -sin(\omega_o - \Omega_L)t \\ 0 \end{pmatrix}, \begin{pmatrix} 0 \\ 0 \\ cos\omega_0 t \end{pmatrix} and \begin{pmatrix} cos(\omega_o + \Omega_L)t \\ sin(\omega_o + \Omega_L)t \\ 0 \end{pmatrix} \tag{35}$$

The physical interpretation of the above solution is presented in section 2.

2. **The calculation of the Landé g factor**

The components of the magnetic moments $\mu_{\mathbf{L}}$and $\mu_{\mathbf{S}}$ combine to give a resultant $\mu_{\mathbf{J}}$ along **J**, which can be expressed by

$$\mu_{\mathbf{J}} = -\mathbf{g}\mu_\beta\mathbf{J} \tag{36}$$

The classical interaction of $\mu_{\mathbf{J}}$ with an applied magnetic field **B** is

$$H = -\mu_{\mathbf{J}}.\mathbf{B} = \mathbf{g}\mu_\beta\mathbf{J}.\mathbf{B} = \mathbf{g}\mu_\beta\mathbf{B}|\mathbf{J}|\mathbf{cos}\theta \tag{37}$$

Where θ is the angle between **J** and **B**. M_J = J, J - 1,..., -J. From the vector model of Fig.1. $cos\theta = M_J|\mathbf{J}|$. Substituting of this value in Eq. 37 gives the allowed Zeeman energies as:

$$E = g\mu_\beta M_J B \tag{38}$$

The well-known formula can be derived from the vector model of Fig.1. For example

$$\mu_{\mathbf{J}} = \mu_{\mathbf{L}}\mathbf{cos}(\mathbf{L},\mathbf{J}) + \mu_{\mathbf{S}}\mathbf{cos}(\mathbf{S},\mathbf{J}) \tag{39}$$

with $\mu_{\mathbf{J}} = \mathbf{g}\mu - \beta\mathbf{J}, \mu_{\mathbf{L}} = \mu_\beta\mathbf{L}$ and $\mu_{\mathbf{S}} = \mathbf{2}\mu_\beta\mathbf{S}$. This gives

$$g = \frac{\mu_\beta\left[Lcos(L,J) + 2Scos(S,J)\right]}{J} \tag{40}$$

From the law of cosine, $cos(\mathbf{L},\mathbf{J}) = (\mathbf{J^2} + \mathbf{L^2} - \mathbf{S^2})/\mathbf{2LJ})$ and $cos(\mathbf{S},\mathbf{J}) = (\mathbf{J^2} + \mathbf{S^2} - \mathbf{L^2})/\mathbf{2SJ}$. Substituting of the eigenvalues $\mathbf{J^2} = \mathbf{j(j+1)}, \mathbf{L^2} = \mathbf{l(l+1)}, \mathbf{S^2} = \mathbf{s(s+1)}$ in the cosines, yields the Landé factor for the atom:

$$g = \frac{3}{2}\frac{s(s+1) - l(l+1)}{2j(j+1)} \tag{41}$$

The physical interpretation of the above formula is presented in section 2.

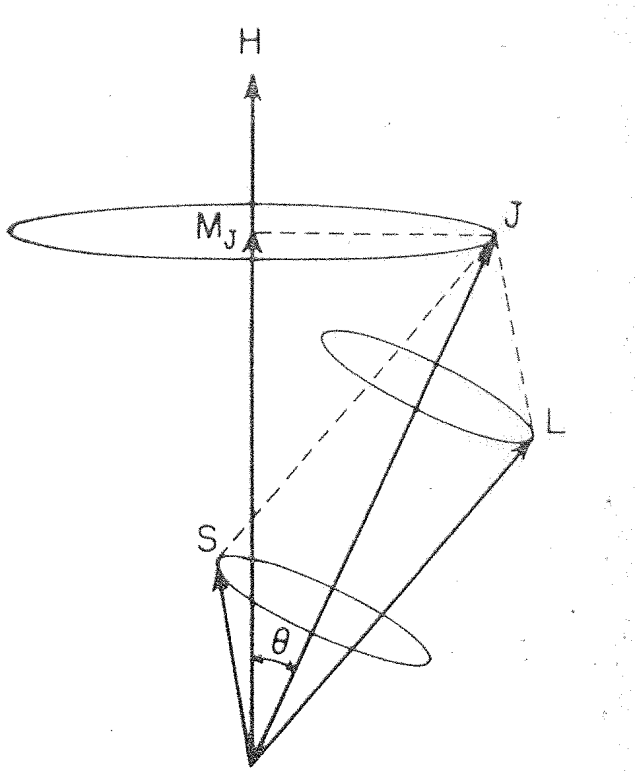

Figure 20: Vector model of an atom in an applied field where there is no nuclear coupling

3. **Time Reversal Symmetry**

Let us first consider the time-dependent Schrödinger equation involving no spin,

$$i\hbar\frac{\partial\psi(t)}{\partial t} = H\psi(t) \tag{42}$$

By denoting the time variable as t' instead of t, the complex conjugate to Eq.42 is

$$-i\hbar\frac{\partial\psi^*(t')}{\partial t'} = H^*\psi^*(t') = H\psi^*(t') \tag{43}$$

in which $H^* = H$ is assumed. Replacing t' by the -t, one obtains

$$i\hbar\frac{\partial\psi^*(-t)}{\partial t} = H\psi^*(-t) \tag{44}$$

which shows that $\psi^*(-t)$ is also the solution of Eq.44. $\psi^*(-t)$ represents the states in which all velocities have opposite directions to those $\psi(t)$. State $\theta\psi(t) \equiv \psi^*(-t)$ is called the time reversed state of $\psi(t)$.

In time-dependent problems, the time-reversed state of $\psi(r)$ is given

$$\theta\psi(r) = K_0\psi(r) = \psi^*(r) \tag{45}$$

K_0 is a time reversal operator for the orbital functions. Using the well-known relation,

$$K_0 Y_{lm}(\theta\varphi) = Y^*_{lm}(\theta\varphi) = (-1)^m Y_{l-m}(\theta\varphi) \tag{46}$$

one can show that the orbital angular momentum operator is transformed byK_0 as

$$K_0\mathbf{I}\mathbf{K_0^{-1}} = -\mathbf{I} \tag{47}$$

which confirms the property of time reversal of K_0. Similarly one can prove the transformation $K_0\mathbf{S}\mathbf{K_O^{-1}} = -\mathbf{S}$